

**KERNFORSCHUNGSZENTRUM
KARLSRUHE**

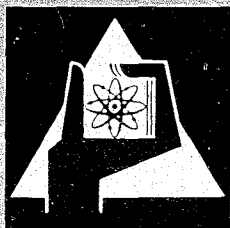
Juli 1968

KFK 792
EUR 3961 e

Institut für Neutronenphysik und Reaktortechnik

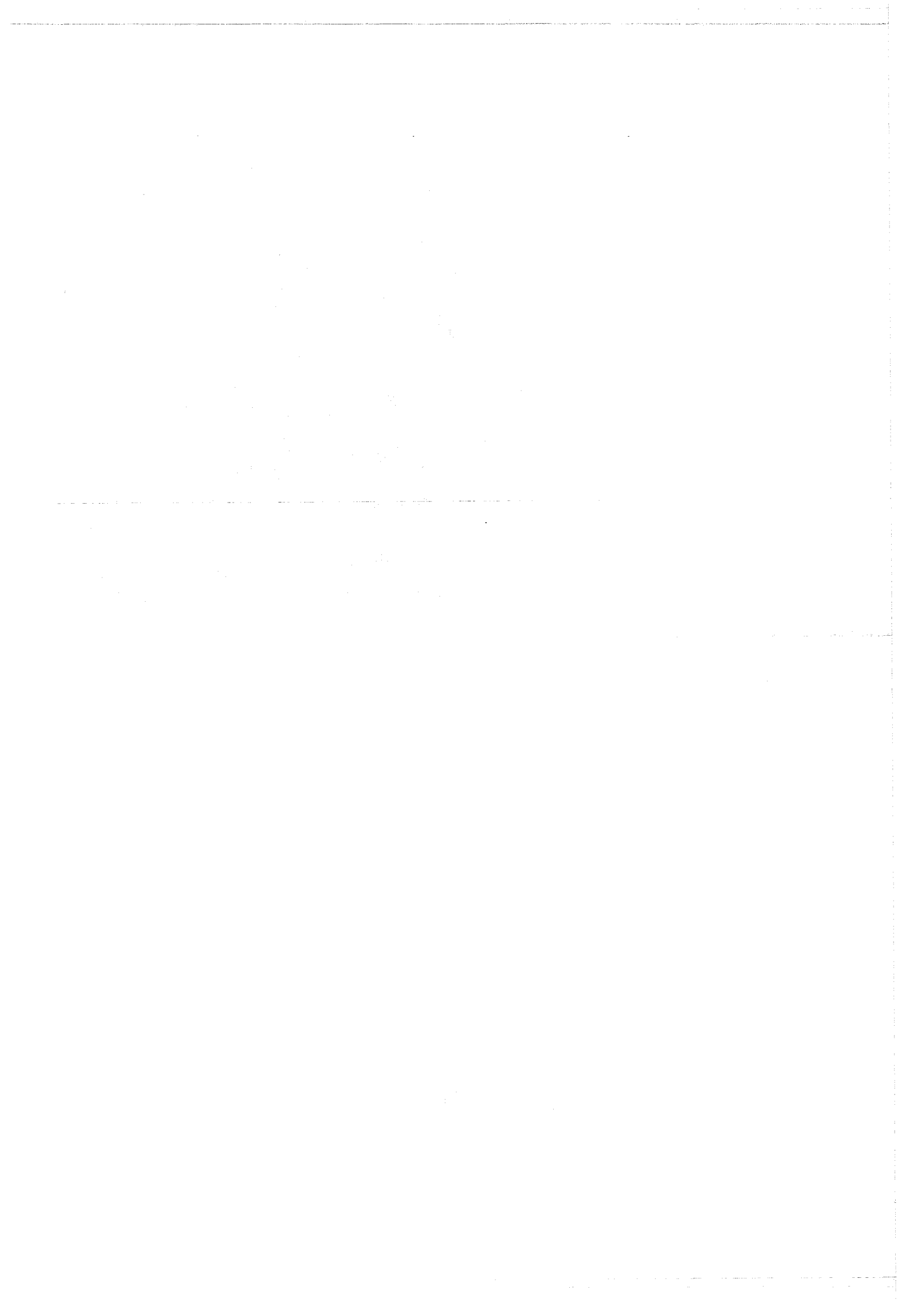
Control Rod Calculations for the Steam
Cooled Fast Breeder Reactor D-1

H. Th. Klippel



GESELLSCHAFT FÜR KERNFORSCHUNG M. B. H.

KARLSRUHE



KERNFORSCHUNGSZENTRUM KARLSRUHE

Juli 1968

KFK 792
EUR 3961 e

Institut für Neutronenphysik und Reaktortechnik

Control Rod Calculations for the Steam
Cooled Fast Breeder Reactor D-1^{KK}

H.Th. Klippel^{KK}

Gesellschaft für Kernforschung mbH., Karlsruhe

^{KK}Work performed within the association in the field of fast reactors between the European Atomic Energy Community and Gesellschaft für Kernforschung mbH., Karlsruhe.

^{KK}Delegated from the Technical University Eindhoven, Netherlands

1. The first part of the document discusses the importance of maintaining accurate records of all transactions and activities. It emphasizes that proper record-keeping is essential for ensuring transparency and accountability in financial reporting.

2. The second part of the document outlines the various methods and techniques used to collect and analyze data. It highlights the need for a systematic approach to data collection and the importance of using reliable sources of information.

3. The third part of the document focuses on the analysis and interpretation of the collected data. It discusses the various statistical and analytical tools used to identify trends, patterns, and relationships within the data.

4. The fourth part of the document addresses the challenges and limitations of data analysis. It discusses the potential for bias, errors, and misinterpretation, and provides strategies to minimize these risks.

5. The fifth part of the document concludes by summarizing the key findings and recommendations. It emphasizes the importance of ongoing monitoring and evaluation to ensure the continued relevance and effectiveness of the data analysis process.

6. The sixth part of the document provides a detailed overview of the data analysis process, including the steps involved in data collection, analysis, and reporting. It also discusses the role of technology in modern data analysis.

7. The seventh part of the document discusses the ethical considerations surrounding data analysis. It emphasizes the need for transparency, privacy, and security in the handling of data, and provides guidelines for ensuring ethical practices.

8. The eighth part of the document provides a detailed overview of the data analysis process, including the steps involved in data collection, analysis, and reporting. It also discusses the role of technology in modern data analysis.

9. The ninth part of the document discusses the ethical considerations surrounding data analysis. It emphasizes the need for transparency, privacy, and security in the handling of data, and provides guidelines for ensuring ethical practices.

10. The tenth part of the document provides a detailed overview of the data analysis process, including the steps involved in data collection, analysis, and reporting. It also discusses the role of technology in modern data analysis.

Contents

Summary

List of Symbols Used

1. Introduction

- 1.1 Purpose of the Study
- 1.2 Core Structure and Control Elements
- 1.3 Methods of Calculation

2. One-Dimensional Calculations

- 2.1 Effectiveness of One Ring of Control Elements
- 2.2 Capture Rate of B^{10} and Power Distribution
for One Absorber Ring
- 2.3 Two Rings of Control Elements
 - 2.3.1 Application of the Perturbation Theory
 - 2.3.2 Effectiveness and Power Distribution for Two Rings
 - 2.3.3 Synthesis Method

3. Two-Dimensional Calculations

- 3.1 Comparison of One and Two-Dimensional Calculations /
Effect of Homogenization
- 3.2 Control Rod Worth for Partially Inserted Rods
- 3.3 Optimum Control of the Critical Reactor
 - 3.3.1 Introduction to the Problem
 - 3.3.2 Quantities Kept Constant in the Calculations
 - 3.3.3 Results
 - 3.3.4 Discussion

4. Conclusion

Acknowledgements

References

Figures

Summary

For the steam cooled fast breeder reactor D-1 the optimization of the location and management of the control elements is performed in a first step.

With one-dimensional diffusion code calculations those locations of one and two rings of control and safety elements are determined which will result in the maximum shutdown reactivity. Perturbation theory provides an expression to calculate the control rod worth of two rings of absorber elements using the results of the calculations for two single rings.

For the optimum ring radii of two rings of control elements that procedure of inserting some control rods a certain depth is determined which maintains the reactor critical with the most favourable power distribution. These calculations are done in two-dimensional ($r-z$) and ($r-\theta$) geometries.

To show the effect of homogenization of the absorber material in a cylindrical ring, some ($r-\theta$) calculations were performed indicating the influence of the absorber rod perimeter on the reactivity worth of the rods.

The calculations were performed with the Karlsruhe Nuclear Program System NUSYS.

List of Symbols Used

- α = Volume fraction of coolant
- β = Volume fraction of cladding and structural material
- ω = Volume fraction of fuel
- ω_{abs} = Volume fraction of absorber material
- ρ = Density (gr/cm³)
- σ = Microscopic cross section (cm²)
- σ^* = Integral microscopic capture rate = $\int_E \sigma_c(E)\phi(E)dE$
- ν = Number of neutrons produced per fission
- Σ = Macroscopic cross section (cm⁻¹)
- ϕ_i = Neutron flux in energy group i
- ϕ = Neutron flux (vector or variable). (n cm⁻² sec⁻¹)
- ϕ_i^+ = Adjoint flux in energy group i
- ϕ^+ = Adjoint flux (vector or variable)
- ϕ^* = Neutron fission weight = $\int_E \phi^+(E)\chi(E)dE$
- $\langle \phi, \phi^+ \rangle$ = Product of flux ϕ and adjoint flux ϕ^+ = $\int_E \phi\phi^+ dE = \text{Sum}_{i=1}^{i=G} \phi_i\phi_i^+$
- θ = Azimuthal angle (angular coordinate)
- χ_i = Fission source distribution

- i, j = Indices for energy groups. $1 \leq i, j \leq G$.
- k_{eff} = Effective multiplication constant
- Δk = Reactivity change or reactivity worth of control elements
- p = Fission density = $\int_E \Sigma_f \phi dE$ (fissions/cm³ sec)
- \hat{p} = Maximum fission density (fissions/cm³ sec)
- \bar{p} = Average fission density (fissions/cm³ sec)
- r = Radial coordinate. (cm)
- y = Ratio of volume fraction of fertile material to the
volume fraction of fissile material = $\frac{U238+Pu240+Pu242}{U235+Pu239+Pu241}$
- B^2 = Buckling (cm⁻²)
- D_i = Diffusion coefficient in energy group i
- D = Thickness of cylindrical ring. (cm)
- E = Neutron energy (eV)
- G = Total number of energy groups
- H = Active absorber length of a control rod (cm)
- M^+ = Transpose of matrix M
- N = Number of control elements in a ring of control elements
- R = Radius of a ring of control elements (cm)
- V = Volume of a reactor zone (cm³)

1. Introduction

1.1 Purpose of the Study

The study, which is described in this report, is based on the design criteria of the steam cooled fast breeder D-1 [1] and deals with the problem of control rod optimization in this fast power reactor.

The purpose of this study is twofold. Primarily, we will try to find that spatial distribution of the 18 control elements that provides the maximal shut - down reactivity. These calculations will be done in a one-dimensional geometry only, mainly for reasons of consumption of computing time. The main aim of this study is not to determine the absolute values of the shut-down reactivity of the control rods, but to show the relative tendencies and to give a physical insight into the problems and results.

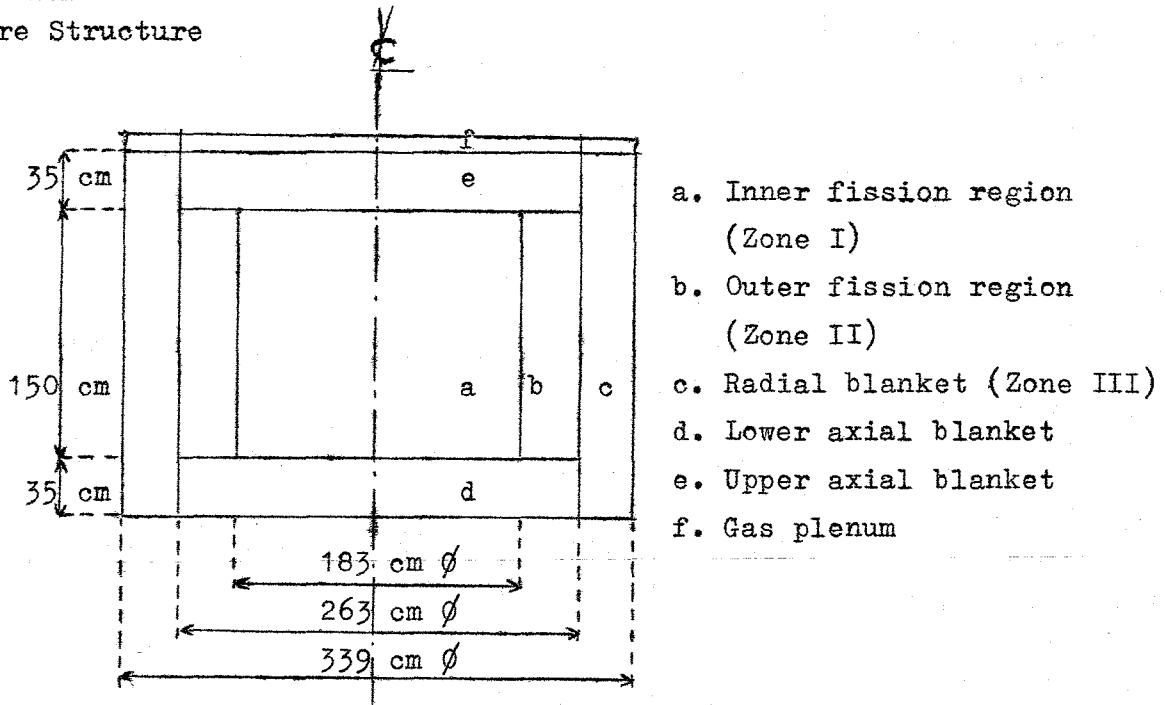
In the second part of this study we will use two-dimensional calculations to find that management of partially inserted control rods which will bring an unperturbed reactor of given excess reactivity down to criticality and, in addition, will allow the maximum power output to be reached. In this way this study also contributes to the design and operating optimization.

1.2 Description of the Core Structure and Control Elements

The cylindrical reactor with an equivalent diameter of 339 cm is loaded with 301 hexagonal elements. The core consists of two concentric fission regions (zone I and II) a radial blanket (zone III) and an upper and lower blanket.

Fig. 1.1 shows the dimensions of the core structure and Table 1.1 gives the volume fractions and some important data for the reactor cell in several reactor regions.

Fig. 1.1
Core Structure



The movable control rods are located within special control elements. (see Fig. 1.2). The control elements are of the same geometric shape as the normal fuel elements. Therefore, they may be placed in any position in the core instead of a fuel element. The reactor design provides for 18 control elements. This number of control elements allows their being distributed in such a way over the reactor that the neutronflux and power peakings can be kept small.

Table 1.1

	Zone I	Zone II	Zone III	Upper blanket	Lower blanket
Number of elements	88	93	120	181	181
Equivalent outer radius (cm)	91.5	131.5	169.5	131.5	131.5
Height (cm)	150	150	220	35	35
Number of fuel pins per fuel element	469	469	169	469	133
Volume fractions per fuel element					
α = fraction of coolant	0.322	0.322	0.241	0.322	0.389
B = fraction of struct. mat. and cladding	0.198	0.198	0.183	0.198	0.168
ω = fraction of fuel	0.480	0.480	0.576	0.480	0.443
Volume fractions per control element					
α = fraction of coolant	0.310	0.310			
B = fraction of struct. mat. and cladding	0.220	0.220			
ω = fraction of fuel	0.308	0.308			
ϵ = fraction of abs absorber mat.	0.162	0.162			
Number of fuel pins per control element	300	300			
Number of absorber pins per contr. el.	19	19			
Fuel enrichment					
$(Pu^9+Pu^1)/(Pu+U)^{tot}$	10.03 ^{a/o}	12.40 ^{a/o}	1.85 ^{a/o}	1.85 ^{a/o}	1.85 ^{a/o}
U-composition U^5/U^8	0 ^{a/o}	0 ^{a/o}	0.004	0.004	0.004 ^{a/o}
$y = \frac{U^8+Pu^0+Pu^2}{U^5+Pu^9+Pu^1}$ v/o	9.32	7.34	43.7	43.7	43.7
Pu-composition a/o Pu ⁹ /Pu ⁰ /Pu ¹ /Pu ²	74/22.7/2.3/1		100/0/0/0	100/0/0/0	100/0/0/0
Burn-up (MWD/tonne)	27,500	27,500	0	0	0
Steam density (g/cm ³) (average)	0.0706	0.0706	0.100	0.0994	0.0503
Struct. material	Inconel 625 8.44 g/cm ³		Incoloy 800 8.01 g/cm ³	Inconel 625 8.44 g/cm ³	

The effective neutron absorber material is B_4C . The lower part of the absorber rods, which is filled with Al_2O_3 , is the follower to retain the same coolant fraction if the control rods are withdrawn. The helium gas released in the $B^{10}(n,\alpha) Li^7$ -process will be stored in the free volumes of the porous carbide.

In the engineering design of a reactor it is not possible to arrange the absorber elements arbitrarily close to each other, because the dimensions of the control rod drive system will limit the minimum distance between two adjacent absorber elements.

In general, however, the minimum pitch of two adjacent absorber elements will be about 20 - 30 cm.

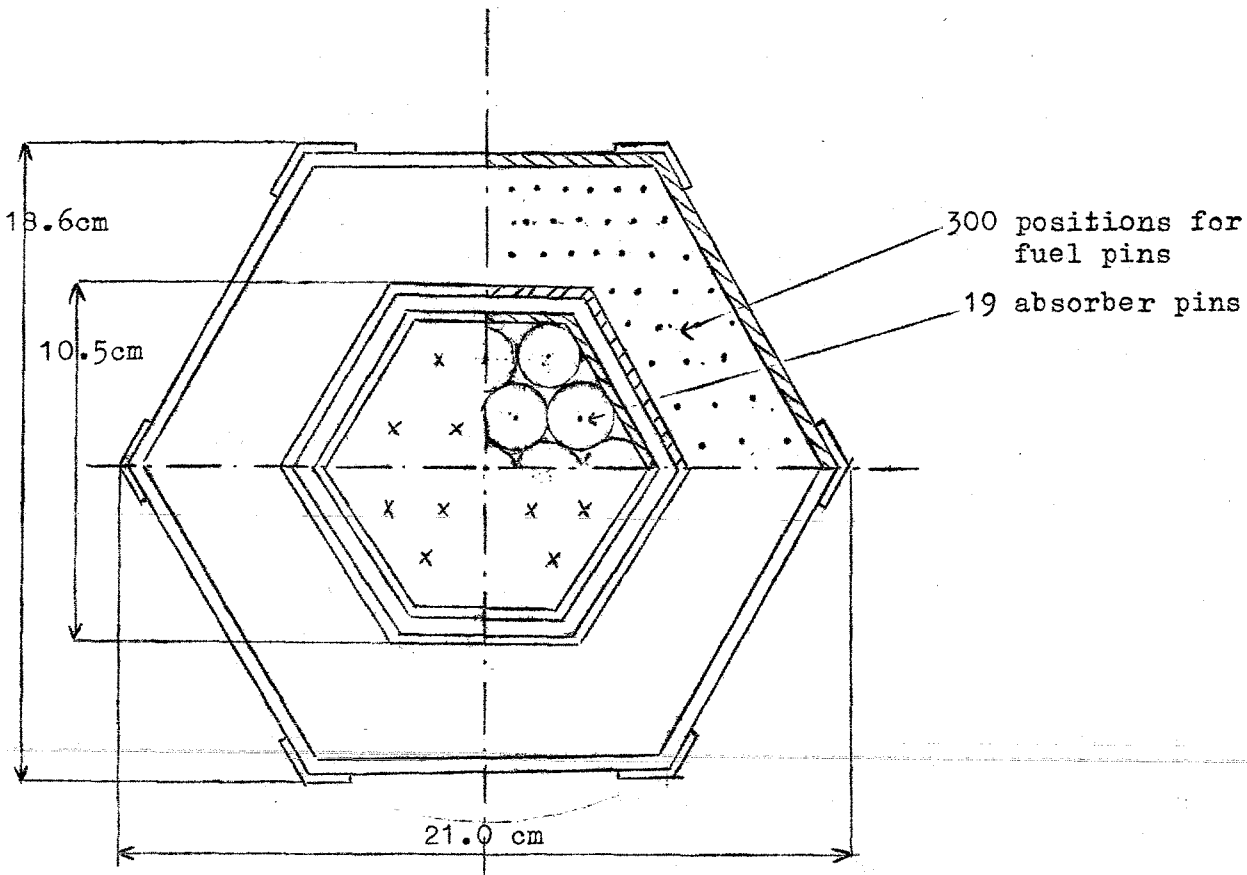
The cross section of the control rod cluster is 95 cm^2 and the volume fractions for the cluster components are as follows:

α	= fraction of coolant	= 0.27
β	= fraction of cladding and structural material	= 0.22
ω_{abs}	= fraction of absorber material	= 0.51

In this study we take the following data for the absorber material:

absorber material	= B_4C
B^{10} enrichment	= 20 % ($B^{10}/B^{11} = 20/80$, natural boron)
absorber density	= 2.50 gr / cm^3
follower material	= Al_2O_3
cladding + structural material	= Inconel 625
effective absorber length	= 100 cm

Fig. 1.2 Control Element



1.3 Methods of Calculation

All reactor calculations are based on multi-group diffusion codes for homogeneous reactor regions. These computer codes are part of the "Karlsruhe Nuclear Programm System NUSYS".

The multigroup diffusion equations have the form

$$-D_i(r)\nabla^2\phi_i(r) + \sum_{rem,i} \Sigma(r)\phi_i(r) = \sum_{j \neq i} \Sigma(r)\phi_j(r) + \frac{\chi_i}{k_{eff}} \sum_j \Sigma_f(r)\phi_j(r)$$

- i, j = indices of the energy groups =
- = 1, 2, 3, ---, G beginning at high energies
- G = number of energy groups

- $\Sigma_{rem,i}$ = neutron removal cross section from group i.
 $\Sigma_{rem,i} = \Sigma_{a,i} + \sum_{j>i} \Sigma_{i \rightarrow j}$
- $\Sigma_{j \rightarrow i}$ = neutron scattering cross section from group j into group i
- D_i = neutron diffusion coefficient
- ϕ_i = neutron flux in group i
- χ_i = fission source distribution
- $\sum_j \nu \Sigma_{f,j} \phi_j$ = fission source

For the cross sections used in the NUSYS system, which are constants in each energy group, a slightly modified ABN-set is used. The energetic self-shielding of the resonances is taken into account by a subprogramm of NUSYS (program 00446). The evaluation code of NUSYS (00447) enables us to calculate the integral fission and capture rates ($\int_E \Sigma_f \phi dE$ and $\int_E \Sigma_c \phi dE$) for each desired isotope as function of the position in the reactor or integrated over the volume of each material zone.

For the two-dimensional calculations a condensation of the 26-group set into a 5-group set is necessary. For the two-dimensional calculations the DIXY program 00940 and the evaluation program 01029 are used.

2. One-Dimensional Calculations

In the one-dimensional calculations for the cylindrical reactor we eliminate the axial and angular coordinates.

In this one-dimensional cylindrical geometry the control elements, which are parallel to the axial z-axis and located on 1 or 2 rings with the "radius" R, are assumed to be smeared-out to cylindrical rings having the same mass of absorber material. Besides, it is possibly only to study fully inserted and completely withdrawn control rings.

Partially inserted control rings can be studied only in the two-dimensional (r-z) geometry.

The "radius" R of the ring is taken as half of the average of the outer and inner diameter of the ring.

Before the study of the inserted and withdrawn control rings it is of interest to know some characteristics of the unperturbed reactor. We will define here the unperturbed reactor as the reactor in which the control elements are replaced by normal fuel elements.

We will use the results of the unperturbed reactor as reference data.

The result of the volume-integrated capture rate of B^{10} as a function of the neutron energy for the unperturbed reactor is given in Fig. 2.1.

The power distribution and the microscopic capture rate of the strong neutron absorber B^{10} as function of the radius will be discussed later on in this report.

For some numerical results of the unperturbed reactor see Table 2.1.

Table 2.1 Numerical Data of the Unperturbed Reactor

Zone	Volume (cm ³) per cm core height	$\int \Sigma_f \phi dE dV$ (fissions per sec)	Maximum fission density \hat{p} (fiss/cm ³ sec)	Average fission density \bar{p} (fiss/cm ³ sec)	Power factor \hat{p}/\bar{p}
I	2.6302 10 ⁴	0.50353	2.0092 10 ⁵	1.914 10 ⁻⁵	1.045
II	2.8023 10 ⁴	0.44462	2.1135 10 ⁵	1.587 10 ⁻⁵	1.332
III	3.5933 10 ⁴	0.05185	3.4070 10 ⁶	1.442 10 ⁻⁶	2.360
I+II	5.4325 10 ⁴	0.94815	2.1135 10 ⁵	1.747 10 ⁻⁵	1.210
I+II+III	9.0258 10 ⁴	1.00000			

2.1 Effectiveness of One Ring of Control Elements

To determine the effectiveness of a ring of control elements it is not sufficient to multiply the $\Delta k(r)$ of a single rod with the number of elements. In the case of multiple control elements, the influence of one rod on the adjacent rods must be considered (mutual shielding or shadowing and flux deformation).

It is known that, with one rod inserted, the flux adjacent to the inserted rod is depressed and the flux elsewhere must be higher to maintain the same integral fission rate. If more rods are close together, they will shadow each other, that is, each rod finds itself partially in the flux depression caused by the other rods, so it absorbs fewer neutrons than it would do in the absence of the other rods. If the rod separation increases, each rod finds itself in the flux peak which occurs beyond the depression and each rod therefore absorbs more neutrons than it would do in the absence of the other rods. However, if we insert the rod too far from the center axis of the core, the effectiveness decreases rapidly, since the flux decreases and disappears at the boundary of the reactor. So, there exists an optimum location of the control rod rings in the reactor.

Table 2.2 contributes some numerical values of the one-dimensional one-ring calculations.

Fig. 2.2 indicates the computed reactivity worth per control element as a function of the radius of the cylindrical absorber ring.

The parameter N is the number of control elements in the ring. For higher numbers of N the optimum radius of the ring increases slightly and the reactivity worth per element decreases. This can be explained as follows:

If for a certain radius of the ring the number of elements in the ring increases, the absorber density increases. (In the actual setup the distance between two control elements will become smaller.) So, shadowing or self-shielding will be stronger for a larger number of control elements. Therefore, the effectiveness for each rod will decrease if the number of control elements in the ring is increased.

Table 2.2 Numerical Data of the One-Dimensional One-Ring Problem

N	R (cm)	$k_{\text{eff}}(\text{Al}_2\text{O}_3)$	$k_{\text{eff}}(\text{B}_4\text{C})$	Δk	$\iint_{\Sigma_c} \Sigma_c^{B10} \phi dE dV$ Vabs ring (B_4C)	$\hat{p}_{\text{I+II}} = \int_{\Sigma_f} \phi dE$ max I, II	$\iint_{\Sigma_f} \phi dE dV$ zone III	$\frac{\hat{p}_{\text{I+II}}}{\bar{p}_{\text{I+II}}}$
3	43.	1.02805	1.01322	0.01483	$4.47088 \cdot 10^{-2}$	$2.30701 \cdot 10^{-5}$	$6.209 \cdot 10^{-2}$	1.339
	64.5	1.02806	1.00882	0.01924	$5.82526 \cdot 10^{-2}$	$2.19185 \cdot 10^{-5}$	$6.037 \cdot 10^{-2}$	1.269
	75.25							
	86.	1.02827	1.00887	0.01940	$6.12781 \cdot 10^{-2}$	$2.41699 \cdot 10^{-5}$	$5.370 \cdot 10^{-2}$	1.389
	97.	1.02793	1.01099	0.01694	$5.52380 \cdot 10^{-2}$	$2.53532 \cdot 10^{-5}$	$4.965 \cdot 10^{-2}$	1.451
	111.5	1.02865	1.01734	0.01131	$4.45577 \cdot 10^{-2}$	$2.42178 \cdot 10^{-5}$	$4.638 \cdot 10^{-2}$	1.380
6	21.5	1.02630	1.01593	0.01037	$3.64063 \cdot 10^{-2}$	$2.33754 \cdot 10^{-5}$	$6.196 \cdot 10^{-2}$	1.355
	43.	1.02601	1.00662	0.01939	$6.11732 \cdot 10^{-2}$	$2.39176 \cdot 10^{-5}$	$6.679 \cdot 10^{-2}$	1.392
	64.5	1.02600	0.99638	0.02962	$9.16411 \cdot 10^{-2}$	$2.25290 \cdot 10^{-5}$	$6.630 \cdot 10^{-2}$	1.307
	75.25	1.02608	0.99368	0.03240	$1.02420 \cdot 10^{-1}$	$2.36010 \cdot 10^{-5}$	$6.141 \cdot 10^{-2}$	1.367
	86.	1.02629	0.99463	0.03166	$1.03461 \cdot 10^{-1}$	$2.81956 \cdot 10^{-5}$	$5.395 \cdot 10^{-2}$	1.620
	97.	1.02559	0.99842	0.02717	$9.34510 \cdot 10^{-2}$	$3.00765 \cdot 10^{-5}$	$4.694 \cdot 10^{-2}$	1.715
	111.5	1.02712	1.00910	0.01802	$7.48573 \cdot 10^{-2}$	$2.77198 \cdot 10^{-5}$	$4.167 \cdot 10^{-2}$	1.570
9	21.5	1.02479	1.01452	0.01027	$3.95889 \cdot 10^{-2}$	$2.36128 \cdot 10^{-5}$	$6.309 \cdot 10^{-2}$	1.370
	43.	1.02413	1.00300	0.02113	$6.98789 \cdot 10^{-2}$	$2.44095 \cdot 10^{-5}$	$6.959 \cdot 10^{-2}$	1.427
	64.5	1.02395	0.98808	0.03587	$1.13511 \cdot 10^{-1}$	$2.31379 \cdot 10^{-5}$	$7.071 \cdot 10^{-2}$	1.353
	75.25	1.02408	0.98309	0.04099	$1.32168 \cdot 10^{-1}$	$2.47987 \cdot 10^{-5}$	$6.465 \cdot 10^{-2}$	1.441
	86.	1.02436	0.98418	0.04018	$1.35570 \cdot 10^{-1}$	$3.16823 \cdot 10^{-5}$	$5.392 \cdot 10^{-2}$	1.820
	97.	1.02336	0.98976	0.03360	$1.21375 \cdot 10^{-1}$	$3.44123 \cdot 10^{-5}$	$4.402 \cdot 10^{-2}$	1.958
	111.5	1.02564	1.00339	0.02225	$9.69017 \cdot 10^{-2}$	$3.06392 \cdot 10^{-5}$	$3.768 \cdot 10^{-2}$	1.730
12	75.25	1.02207	0.97480	0.04727	$1.55207 \cdot 10^{-1}$	$2.57568 \cdot 10^{-5}$	$6.740 \cdot 10^{-2}$	1.499
	86.	1.02249	0.97624	0.04625	$1.61053 \cdot 10^{-1}$	$3.42428 \cdot 10^{-5}$	$5.442 \cdot 10^{-2}$	1.970
	97.	1.02117	0.98350	0.03767	$1.42615 \cdot 10^{-1}$	$3.81822 \cdot 10^{-5}$	$4.123 \cdot 10^{-2}$	2.165
	111.5	1.02417	0.99921	0.02496	$1.13508 \cdot 10^{-1}$	$3.31000 \cdot 10^{-5}$	$3.428 \cdot 10^{-2}$	1.864

It is evident that the density of the absorber material in the homogenized absorber ring decreases with increasing radius of the absorber ring, keeping the thickness of the ring constant. For this reason, the optimum radius will shift to higher values with increasing number of elements in the ring.

Fig. 2.2 shows that the optimum radius changed from $R = 75$ cm (3 control elements in the absorber ring) to $R = 80$ cm (12 control elements in the absorber ring). The calculations are done for a ring thickness of 11 cm. The ring thickness is about the same as the diameter of one absorber pin cluster. The homogeneous ring consists of fuel, coolant, cladding and structural material, and absorber material with volume fractions which are modifications of those shown in Table 1.1, but in such a way that the total absorber material in a ring will be constant and independent of the absorber ring radius.

2.2 Capture Rate of B^{10} and Power Distribution for One Absorber Ring

To study the effect of the neutron absorption in B^{10} we calculate the integral microscopic capture rate $\sigma^{\#}(r) = \int_E \sigma_c^{B^{10}}(E, r) \phi(E, r) dE$ as a function of the position in the reactor.

As expected we find a depression of the capture rate near the absorber ring and elsewhere the capture rate can even be higher than in the unperturbed case because of the normalization which provides no change in the total power. As we will see in Chapter 2.3.1 the radial dependence of the capture rate of B^{10} is a quantity to determine approximately the effectiveness Δk in the case of two rings of absorber elements.

If we take the example of the ring radius $R = 43.0$ cm (Fig. 2.3) we see that the capture rate $\sigma^{\#}$ near the boundary of zone I and zone II is higher than for the unperturbed reactor (with $N = 0$). The increase in the capture rate in the blanket zone at the core-blanket interface is due to the spectrum softening and the high absorption cross section of B^{10} in the low neutron energy range. For higher values of the ring radius (for example $R = 97.0$ in Fig. 2.4) we see that the capture rate $\sigma^{\#}$ in Zone II will be lower than for the unperturbed reactor.

The analogous arguments as for the flux depression and the flux increase can be applied to the power distribution; See Fig. 2.5 and Fig. 2.6 which give the fission distribution, $p = \int_E \Sigma_f \phi dE$ as a function of the radius. ($p = \text{fissions/sec cm}^3$)

It will be noted that the distributions are normalized to one fission/sec over the complete reactor.

An integral quantity which characterizes the radial power distribution is the radial power factor \hat{p}/\bar{p} . It is defined as the ratio of radial peak to radial average fission density in the core. For the radial average fission density we take the average value of the density in zone I and zone II (we note that only about 5% of the fissions occurs in the blanket).

It is seen from Table 2.2 that the optimum power factor (lowest peak-to-average ratio) appears for absorber rings with a radius of about 65 cm, which is not far from the ring radius with optimum absorber effectiveness. This is mainly due to the fact that for a ring radius near the radius with optimum absorber effectiveness the flux distribution will be more favourable and hence the power distribution will be fairly good.

2.3 Two Rings of Control Elements

2.3.1 Application of the Perturbation Theory

For the following we start from the multigroup diffusion equation for a multiplying system.

$$-D_i \nabla^2 \phi_i + \Sigma_{\text{rem},i} \phi_i = \sum_{j \neq i} \Sigma_{j \rightarrow i} \phi_j + \frac{\lambda_i}{k_{\text{eff}}} \sum_j (\nu \Sigma_f)_j \phi_j \quad (1)$$

i, j are indices of energy groups, see Chapter 1.5. As usual, we assume that the fission spectrum is independent of energy of the neutron which induces the fission. The normal boundary conditions will be fulfilled. In operator form we write (1) as follows:

$$M \phi = \frac{1}{k_{\text{eff}}} \chi \langle \nu \Sigma_f, \phi \rangle \quad (2)$$

$\phi, \chi, \nu \Sigma_f$ are vectors,

M is a matrix with the elements

$$M_{ii} = -D_i \nabla^2 + \Sigma_{\text{rem},i}$$

$$M_{ij} = -\Sigma_{j \rightarrow i} \quad (j < i)$$

$$M_{ji} = 0 \quad (j < i)$$

$$\begin{aligned} \langle \nu \Sigma_f, \phi \rangle &= \text{scalar product} = \\ &= \sum_j (\nu \Sigma_f)_j \phi_j = \int_E \nu \Sigma_f(E) \phi(E) dE \end{aligned}$$

In the perturbation theory formalism we have to take the adjoint flux ϕ^+ and the adjoint operator M^+ . M^+ is defined by

$$\int (\psi M \phi - \phi M^+ \psi) dV = 0 \quad (3)$$

in which ψ and ϕ are functions with the boundary condition that ψ and ϕ vanish at the extrapolated surface of the reactor volume.

ϕ^+ is the solution of the adjoint equation

$$-D_i \nabla^2 \psi_i + \Sigma_{\text{rem},i} \psi_i = \sum_{j \neq i} \Sigma_{i \rightarrow j} \psi_j + \frac{(\nu \Sigma_f)_i}{k_{\text{eff}}} \sum_j \chi_j \psi_j \quad (4)$$

In the matrix form we have from (4)

$$M^+ \psi = \frac{\nu \Sigma_f}{k_{\text{eff}}} \langle \chi, \psi \rangle \quad (5)$$

with $M_{ij}^+ = M_{ji}$.

The adjoint operator M^+ is the transpose of the matrix M.

Equation (3) is satisfied by the solutions of (2) and (5).

Equation (5) can be written also as

$$\phi^+ M = \frac{\nu \Sigma_f}{k_{\text{eff}}} \langle \phi^+, \chi \rangle \quad (6)$$

where $\phi_i^+ = \psi_i$.

Now we write (2) and (6), respectively, for two different conditions a and b of the system.

$$M_a \phi_a = \frac{1}{k_{\text{eff}a}} \chi \langle \nu_{\Sigma_{fa}}, \phi_a \rangle \quad (7)$$

$$\phi_b^+ M_b = \frac{1}{k_{\text{eff}b}} \nu_{\Sigma_{fb}} \langle \phi_b^+, \chi \rangle \quad (8)$$

(7) and (8) can be transformed into

$$-\int \langle \phi_b^+, (M_b - M_a) \phi_a \rangle dV = \int \langle \phi_b^+, \chi \rangle \left[\frac{\langle \nu_{\Sigma_{fa}}, \phi_a \rangle}{k_{\text{eff}a}} - \frac{\langle \nu_{\Sigma_{fb}}, \phi_a \rangle}{k_{\text{eff}b}} \right] dV \quad (9)$$

The integration is done over the total volume of the reactor.

With $M_b = M_a + \delta M$

and $\nu_{\Sigma_{fb}} = \nu_{\Sigma_{fa}} + \delta \nu_{\Sigma_f}$

we obtain:

$$\begin{aligned} & -\int \langle \phi_b^+, \delta M \phi_a \rangle dV + \int \frac{\langle \phi_b^+, \chi \rangle \langle \delta \nu_{\Sigma_f}, \phi_a \rangle}{k_{\text{eff}b}} dV = \\ & = \int \langle \phi_b^+, \chi \rangle \langle \nu_{\Sigma_{fa}}, \phi_a \rangle \left[\frac{1}{k_a} - \frac{1}{k_b} \right] dV \end{aligned} \quad (10)$$

Near criticality we can write

$$\frac{1}{k_a} - \frac{1}{k_b} \approx k_b - k_a = \delta k$$

$$\delta k = \frac{-\int \langle \phi_b^+, \delta M \phi_a \rangle dV + \frac{1}{k_b} \int \langle \phi_b^+, \chi \rangle \langle \delta \nu_{\Sigma_f}, \phi_a \rangle dV}{\int \langle \phi_b^+, \chi \rangle \langle \nu_{\Sigma_{fa}}, \phi_a \rangle dV} \quad (11)$$

In this study we take condition a as the reactor with inserted B_4C rods and condition b as the reactor in which the control rods are withdrawn and the Al_2O_3 followers are used instead of B_4C . This means that the

fission cross sections are not changed, so (11) reduces to

$$\delta k = \frac{-\int \langle \phi_{A1}^+, \delta M \phi_B \rangle dV}{\int \langle \phi_{A1}^+, \chi \rangle \langle \nu \Sigma_f, \phi_B \rangle dV} \quad (12)$$

(The influence of the change in resonance self - shielding can be neglected).

We now examine the reactor with three types of control rod configurations.

Configuration 1: Only one ring of N_1 control elements at radius R_1 .

Configuration 2: Only one ring of N_2 control elements at radius R_2 .

Configuration 12: One ring of N_1 control elements at radius R_1 and a second ring of N_2 control elements at radius R_2 .

With the definition of control rod effectiveness

$$\Delta k = k_{\text{eff}}(A1_2 O_3) - k_{\text{eff}}(B_4 C)$$

we obtain from (12)

$$\Delta k_{12} = - \frac{\int \langle \phi_{12A1}^+, \Delta M_{12} \phi_{12B} \rangle dV}{\int \langle \phi_{12A1}^+, \chi \rangle \langle \nu \Sigma_{f12}, \phi_{12B} \rangle dV} \quad (13)$$

$$\Delta k_1 = - \frac{\int \langle \phi_{1A1}^+, \Delta M_1 \phi_{1B} \rangle dV}{\int \langle \phi_{1A1}^+, \chi \rangle \langle \nu \Sigma_{f1}, \phi_{1B} \rangle dV} \quad (14)$$

$$\Delta k_2 = - \frac{\int \langle \phi_{2A1}^+, \Delta M_2 \phi_{2B} \rangle dV}{\int \langle \phi_{2A1}^+, \chi \rangle \langle \nu \Sigma_{f2}, \phi_{2B} \rangle dV} \quad (15)$$

It is clear that the control rod regions are the only regions where the matrix elements will be perturbed.

With a rearrangement of (13) (14) (15) we obtain in one-group theory:

$$\Delta k_{12} F_{12} = \Delta k_1 F_1 \left(\frac{\phi_{12A1}^+}{\phi_{1A1}^+} \right)_{R_1} \left(\frac{\phi_{12B}}{\phi_{1B}} \right)_{R_1} + \Delta k_2 F_2 \left(\frac{\phi_{12A1}^+}{\phi_{2A1}^+} \right)_{R_2} \left(\frac{\phi_{12B}}{\phi_{2B}} \right)_{R_2} \quad (16)$$

In this expression we have the following notations:

$$F_{12} = \int \langle \phi_{12A1}^+, \chi \rangle \langle \nu \Sigma_{f12}, \phi_{12B} \rangle dV$$

$$F_1 = \int \langle \phi_{1A1}^+, \chi \rangle \langle \nu \Sigma_{f1}, \phi_{1B} \rangle dV$$

$$F_2 = \int \langle \phi_{2A1}^+, \chi \rangle \langle \nu \Sigma_{f2}, \phi_{2B} \rangle dV$$

$$\left(\frac{\phi_{12A1}^+}{\phi_{1A1}^+} \right)_{R_1} = \text{average value of } \frac{\phi_{12A1}^+}{\phi_{1A1}^+} \text{ over the control rods with radius } R_1.$$

With expression (16) we have a formalism to obtain the control rod effectiveness of two rings of control elements if we know the rod effectiveness of two systems with a single control ring. To obtain a manageable formalism (it is very lengthy to calculate the F factor), we use the following approximation:

$$F_{12} \approx F_1 \approx F_2. \quad *)$$

*) To confirm this approximation we have calculated the F-factors for the configuration $N_1 = 6$, $N_2 = 12$.

$$R_1 = 21,5 \text{ cm} \quad R_2 = 97 \text{ cm} \quad \frac{F_1}{F_{12}} = 0.980 \quad \frac{F_2}{F_{12}} = 1.093$$

$$R_1 = 43 \text{ cm} \quad R_2 = 97 \text{ cm} \quad \frac{F_1}{F_{12}} = 0.990 \quad \frac{F_2}{F_{12}} = 1.120$$

$$R_1 = 64,5 \text{ cm} \quad R_2 = 97 \text{ cm} \quad \frac{F_1}{F_{12}} = 0.917 \quad \frac{F_2}{F_{12}} = 1.032$$

If we proceed from the result of one-group theory (Eq.(16)) to multi-group theory, it is evident to assume the following equivalence:

$$\frac{\phi_{12A1}^+}{\phi_{1A1}^+ R_1} \longrightarrow \frac{\langle \phi_{12A1}^+(R_1), \chi(R_1) \rangle}{\langle \phi_{1A1}^+(R_1), \chi(R_1) \rangle}$$

$$\frac{\phi_{12B}}{\phi_{1B} R_1} \longrightarrow \frac{\langle \sigma_{c12}^{B10}(R_1), \phi_{12B}(R_1) \rangle}{\langle \sigma_{c1}^{B10}(R_1), \phi_{1B}(R_1) \rangle}$$

With these assumptions we obtain from (16)

$$\Delta k_{12} = \Delta k_1 \frac{\phi_{12A1}^{\#}(R_1) \sigma_{12B}^{\#}(R_1)}{\phi_{1A1}^{\#}(R_1) \sigma_{1B}^{\#}(R_1)} + \Delta k_2 \frac{\phi_{12A1}^{\#}(R_2) \sigma_{12B}^{\#}(R_2)}{\phi_{2A1}^{\#}(R_2) \sigma_{2B}^{\#}(R_2)} \quad (17)$$

in which:

$$\phi_{12A1}^{\#}(R_1) = \int_E \phi_{12A1}^{\#} \chi \, dE \quad = \text{neutron fission weight at position of the control rod with radius } R_1 \text{ in the configuration of two rings with control rods withdrawn.}$$

$$\phi_{1A1}^{\#}(R_1) = \int_E \phi_{1A1}^+ \chi \, dE \quad = \text{neutron fission weight at position of the control rod with radius } R_1 \text{ in the configuration of one ring with withdrawn rods.}$$

$$\sigma_{12B}^{\#}(R_1) = \int_E \sigma_{c12}^{B10} \phi \, dE \quad = \text{capture rate of } B^{10} \text{ at the position of the control rod with radius } R_1 \text{ in the configuration of two rings with inserted rods.}$$

$$\sigma_{1B}^{\#}(R_1) = \int_E \sigma_{c1}^{B10} \phi \, dE \quad = \text{capture rate of } B^{10} \text{ at the position of the control rod with radius } R_1 \text{ in the configuration of one ring with inserted rods.}$$

etc.

If we change the conditions a and b in (11) so that condition b is the reactor with B_4C rods inserted and condition a is the reactor with control rods withdrawn (Al_2O_3 followers inserted), we obtain a similar equation

$$\Delta k_{12} = \Delta k_1 \frac{\phi_{12B}^{\#}(R_1)}{\phi_{1B}^{\#}(R_1)} \frac{\sigma_{12Al}^{\#}(R_1)}{\sigma_{1Al}^{\#}(R_1)} + \Delta k_2 \frac{\phi_{12B}^{\#}(R_2)}{\phi_{2B}^{\#}(R_2)} \frac{\sigma_{12Al}^{\#}(R_2)}{\sigma_{2Al}^{\#}(R_2)} \quad (18)$$

2.3.2 Effectiveness and Power Distribution for Two Rings

In this study we locate the 18 elements within two rings of control elements. For reasons of symmetry we examine only the following two possibilities:

- a. Inner ring of 6 elements, outer ring of 12 elements.
- b. Inner ring of 9 elements, outer ring of 9 elements.

The radius R_1 of the inner ring and the radius R_2 of the outer ring are variable parameters. Fig. 2.7 and Fig. 2.8 show the radial distribution of the B^{10} capture rate $\int_E \sigma_c \phi dE$ and the fission density $\int_E \Sigma_f \phi dE$ for a certain location of the two rings. If we compare the figures with those of the one-ring problem we see the very important effect of the additional ring on the radial distributions.

To show the validity of Eq. (16) in one case we calculated Δk_{12} from Eq. (16) for various positions of the inner ring with a constant radius of the second ring ($R_2 = 97$ cm). In Table 2.3 this value Δk_{12} is compared with the exact results of the computer calculations Δk_{exact} . It is seen that the perturbation formalism overestimates the reactivity worth by about 5%. Since we know that the total effectiveness of 18 rods is about $\Delta k \approx 0.075$, it is very probable that the difference between Δk_{12} and Δk_{exact} (which is about 0.004) will be small compared to the uncertainty which arises from the application of the homogeneous diffusion theory to the determination of the control rod worth. For the simpler equation (17) we obtain a difference from - 2% to 10%. Fig. 2.9 and Table 2.4 gives the total reactivity worth Δk_{exact} of two rings of control elements as a function of the radius of the inner absorber ring. The parameter is the thickness of the absorber ring. It is seen that the position of the inner ring for a maximum Δk is independent of the ring thickness.

Table 2.3

Ratio of the reactivity worth from direct calculations and perturbation theory as function of the radius of the inner absorber ring.

$\frac{\Delta k_{12}}{\Delta k_{\text{exact}}}$	R_1		
	21,5 cm	43 cm	64,5 cm
A	0.983	0.990	1.070
B	1.043	1.058	1.042

$$A) \Delta k_{12} = \frac{\phi_{12A1}^*(R_1)}{\phi_{1A1}^*(R_1)} \frac{\sigma_{12B}^*(R_1)}{\sigma_{1B}^*(R_1)} \Delta k_1$$

$$+ \frac{\phi_{12A1}^*(R_2)}{\phi_{2A1}^*(R_2)} \frac{\sigma_{12B}^*(R_2)}{\sigma_{2B}^*(R_2)} \Delta k_2$$

$$B) \Delta k_{12} = \frac{F_1}{F_{12}} \frac{\phi_{12A1}^*(R_1)}{\phi_{1A1}^*(R_1)} \frac{\sigma_{12B}^*(R_1)}{\sigma_{1B}^*(R_1)} \Delta k_1$$

$$+ \frac{F_2}{F_{12}} \frac{\phi_{12A1}^*(R_2)}{\phi_{2A1}^*(R_2)} \frac{\sigma_{12B}^*(R_2)}{\sigma_{2B}^*(R_2)} \Delta k_2$$

Table 2.4 One-Dimensional Two-Ring Problem

$R_1(N_1=6)$ =variable, $R_2(N_2=12)$ = interface zone I-zone II

D (cm)	R_1 (cm)	$k(\text{Al}_2\text{O}_3)$	$k(\text{B}_4\text{C})$	Δk	$\iint_{V_{\text{abs1}}} \Sigma_c^{B^{10}} \phi dE dV$ (capt/sec)	$\iint_{V_{\text{abs2}}} \Sigma_c^{B^{10}} \phi dE dV$ (capt/sec)	$\int_{V_{\text{zone III}}} dV \int_E \Sigma_f \phi dE$	$\hat{p}_{\text{I+II}}$ (fissions/ cm^3/s)	$\frac{\hat{p}_{\text{I+II}}}{\bar{p}_{\text{I+II}}}$
11	21.5	1.0164	0.9470	0.0694	$6.107_{10^{-2}}$	$1.795_{10^{-1}}$	$6.316_{10^{-2}}$	$2.382_{10^{-5}}$	1.380
	43.0	1.0162	0.9327	0.0835	$9.665_{10^{-2}}$	$1.843_{10^{-1}}$	$7.092_{10^{-2}}$	$2.202_{10^{-5}}$	1.287
	64.5	1.0166	0.9413	0.0753	$1.226_{10^{-1}}$	$1.493_{10^{-1}}$	$5.572_{10^{-2}}$	$4.396_{10^{-5}}$	2.527
	75.25	1.0169	0.9539	0.0630	$1.116_{10^{-1}}$	$1.291_{10^{-1}}$	$4.479_{10^{-2}}$	$4.923_{10^{-5}}$	2.800
5	21.5	1.0162	0.9514	0.0648	$5.332_{10^{-2}}$	$1.672_{10^{-1}}$	$6.644_{10^{-2}}$	$2.241_{10^{-5}}$	1.302
	43.0	1.0159	0.9394	0.0765	$8.405_{10^{-2}}$	$1.695_{10^{-1}}$	$7.340_{10^{-2}}$	$2.096_{10^{-5}}$	1.228
	64.5	1.0162	0.9459	0.0703	$1.067_{10^{-1}}$	$1.421_{10^{-1}}$	$5.982_{10^{-2}}$	$4.003_{10^{-5}}$	2.310
	75.25	1.0166	0.9563	0.0603	$9.937_{10^{-2}}$	$1.261_{10^{-1}}$	$4.984_{10^{-2}}$	$4.519_{10^{-5}}$	2.582

Normalization: $\int_{V_{\text{I+II+III}}} dV \int_E \Sigma_f \phi dE = 1$ (fissions/sec)

2.3.3 Synthesis Method

As we have seen in Table 2.3, the equations of Chapter 2.3.1 are applicable to estimate the effectiveness of the insertion of two rings of control elements into the reactor. This will be especially important if one wishes to determine the ring radii for which the absorber rings have the maximum reactivity worth. To estimate the positions for maximum effectiveness we would have to perform many computer calculations in which the ring radii have to be varied. This will take too much computing time. With the aid of the solutions of Chapter 2.3.1, however, it is possible to calculate the optimum ring radii for the two-ring problem with the results of the one-ring problem, so we can reduce the expensive computer calculations. With reference to the capture rate distribution $\sigma_o^{\#}(r) = \int_E \sigma_c^{B10}(E,r) \phi(E,r) dE$ of the unperturbed reactor we approximate the capture rate distribution for the two-ring problem $\sigma_{12}^{\#}(r)$ by:

$$\frac{\sigma_{12}^{\#}(r)}{\sigma_o^{\#}(r)} = \frac{\sigma_1^{\#}(r)}{\sigma_o^{\#}(r)} \cdot \frac{\sigma_2^{\#}(r)}{\sigma_o^{\#}(r)} \quad (1)$$

where

- $\sigma_o^{\#}(r)$ = capture rate $\int \sigma_c \phi dE$ at position r in the unperturbed reactor.
- $\sigma_1^{\#}(r)$ = capture rate $\int \sigma_c \phi dE$ at position r in the reactor with a single absorber ring at radius R_1 .
- $\sigma_2^{\#}(r)$ = capture rate $\int \sigma_c \phi dE$ at position r in the reactor with a single absorber ring at radius R_2 .
- $\sigma_{12}^{\#}(r)$ = capture rate $\int \sigma_c \phi dE$ at position r in the reactor with one ring at R_1 and a second ring at R_2 .

To show the quality of this approximation we have plotted for one special case in Fig. 2.10 the direct result $\frac{\sigma_{12}^{\#}(r)}{\sigma_o^{\#}(r)}$ from the exact two-ring problem $R_1(N_1=6)=43.0, R_2(N_2=12)=97.0$ and the approximation $\frac{\sigma_1^{\#}(r)}{\sigma_o^{\#}(r)} \cdot \frac{\sigma_2^{\#}(r)}{\sigma_o^{\#}(r)}$

from the two single ring problems $R(N=6)=43.0$ cm and $R(N=12)=97.0$ cm. (see also Fig. 2.3 and Fig. 2.4).

In the same way as for the capture rate distribution we approximate the fission neutron weight $\phi_{12}^{\#}(r) = \int_E \phi^+ \chi \, dE$ by

$$\frac{\phi_{12}^{\#}(r)}{\phi_0^{\#}(r)} = \frac{\phi_1^{\#}(r)}{\phi_0^{\#}(r)} \cdot \frac{\phi_2^{\#}(r)}{\phi_0^{\#}(r)} \quad (2)$$

See also Fig. 2.11 in which we see that the approximation corresponds to the exact distribution within 2 %.

With (1) and (2) we write Eq. (16) of Chapter 2.3.1

$$\Delta k_{12} = \Delta k_1 \frac{\phi_{2A1}^{\#}(R_1)}{\phi_0^{\#}(R_1)} \frac{\sigma_{2B}^{\#}(R_1)}{\sigma_0^{\#}(R_1)} + \Delta k_2 \frac{\phi_{1A1}^{\#}(R_2)}{\phi_0^{\#}(R_2)} \frac{\sigma_{1B}^{\#}(R_2)}{\sigma_0^{\#}(R_2)} \quad (3)$$

With this equation we can estimate the absorber effectiveness of two rings of control rods using the results of the calculations for two single rings.

With Equation (3) we have calculated Δk_{12} as a function of the ring radius R_1 for various positions of the outer absorber ring. Fig. 2.12 shows $\Delta k_{12}(R_1)$ for the condition with 6 absorber elements in the inner ring ($N_1=6$) and 12 absorber elements in the outer ring ($N_2=12$).

To determine the optimum ring radii, for which Δk_{12} has a maximum, we plotted in Fig. 2.13 $\Delta k_{12 \text{ max.}}$, the maximum value of $\Delta k_{12}(R_1)$, (that means at the optimum value of R_1) as a function of the ring radius R_2 . The ring radius R_2 for which $\Delta k_{12 \text{ max.}}$ has an extremum gives us the optimum position of the outer absorber ring.

From Fig. 2.13 we can conclude that the optimum position of the outer absorber ring is close to the boundary of the first and second fission region. The optimum inner ring radius consequently will be about 57 cm. ($\Delta k_{12 \text{ exact}}$ gives an optimum of $R_{1 \text{ opt.}} \approx 50$ cm); See also Fig. 2.14 in which $R_{1 \text{ max.}}$ is given as a function of R_2 . $R_{1 \text{ max.}}$ is defined as the ring radius R_1 for which $\Delta k_{12}(R_1)$ has the maximum value $\Delta k_{12 \text{ max.}}$.

It will be noted here that near the optimum inner ring radius the reactivity worth Δk varies slowly with R_1 . Therefore, a small deviation of the inner ring radius from the optimum radius is allowed.

As we saw in Chapter 1.2 the distance of two adjacent absorber elements should be larger than 30 cm.

For a ring of absorber elements of radius 50 cm the distance in the azimuthal direction between two adjacent absorber elements will be about 52 cm for 6 absorber elements in the ring and about 35 cm for 9 absorber elements in the ring. Therefore, the results of this chapter match the requirement of engineering design.

This is true also for the outer ring at a radius of about 95 cm and for the radial distance between both rings.

3. Two-Dimensional Calculations

3.1 Comparison of One and Two-Dimensional Calculations /

Effect of Homogenization

In the preceding chapter we studied the one-dimensional problem. Now we will show the effect of the homogeneous ring on the worth of the control rods as a function of ring thickness and compare this with two-dimensional ($r - \theta$) calculations.

In Fig. 2.9 the reactivity worth Δk was given for the ring thickness 5 and 11 cm, as a function of the inner ring radius. We concluded, that the ring thickness has no influence on the determination of the optimum ring radius. Only the absolute value of the reactivity worth will decrease for a smaller ring thickness, keeping the total amount of absorber material constant.

Table 3.1 shows this effect in the one-dimensional geometry, (this is for fixed radii).

We see that Δk and the integral absorption rate $\iint \Sigma_c^{B^{10}} \phi dE dV$ of B^{10} in the absorber rings depend nearly linearly on the ring thickness in the range studied. This fact can be explained as follows:

The volume of an absorber ring depends nearly linearly on the ring thickness, i.e. the macroscopic cross section Σ_c of B^{10} in the ring will be inversely proportional to the ring thickness. The shadowing

(or flux depression) in a ring of smaller ring thickness is stronger than for a larger ring thickness
(roughly proportional to Σ_c of B^{10}).

The criticality change will be approximately inversely proportional to the flux depression, which explains the behaviour just mentioned. In the same way of arguing one may state that the integral B^{10} capture rate $\iint \Sigma_c \phi dE dV$ decreases and, consequently, the reactivity worth Δk will be lower for smaller ring thickness.

In some $(r - \theta)$ calculations (θ is the azimuthal angle with respect to the axis of the core) we studied the effect of the rod perimeter as a measure of the rod surface on the control rod worth.

Table 3.1

One-Dimensional Problem $R_1(N_1=6)=43.0$ $R_2(N_2=12)$ at interface of zone I-zone II

D (cm)	$k(\text{Al}_2\text{O}_3)$	$k(\text{B}_4\text{C})$	Δk	$\iint \Sigma_c^{B^{10}} \phi dE dV$			$\iint \Sigma_f \phi dE dV$		
				abs 1	abs 2	captures sec	zone I	zone II	fissions sec
11	1.0162	0.9327	0.0835	$9.665_{10^{-2}}$	$1.843_{10^{-1}}$	$2.810_{10^{-1}}$	0.4826	0.4465	0.0709
5	1.0159	0.9394	0.0765	$8.405_{10^{-2}}$	$1.695_{10^{-1}}$	$2.536_{10^{-1}}$	0.4575	0.4691	0.0734
2	1.0167	0.9437	0.0730	$7.828_{10^{-2}}$	$1.613_{10^{-1}}$	$2.396_{10^{-1}}$	0.4450	0.4810	0.0740
(r- θ)	1.0170	0.9548	0.0622	$7.172_{10^{-2}}$	$1.353_{10^{-1}}$	$2.070_{10^{-1}}$	0.4794	0.4542	0.0664

D (cm)	\hat{P}_I fissions/cm ³ s	\hat{P}_{II} fissions/cm ³ s	$\frac{\hat{P}_I}{\bar{P}_I}$	$\frac{\hat{P}_{II}}{\bar{P}_{II}}$	$\frac{\hat{P}_{I+II}}{\bar{P}_{I+II}}$
11	$2.2020_{10^{-5}}$	$1.8571_{10^{-5}}$	1.200	1.164	1.287
5	$2.0964_{10^{-5}}$	$1.9800_{10^{-5}}$	1.206	1.183	1.228
2	$2.0396_{10^{-5}}$	$2.0304_{10^{-5}}$	1.200	1.182	1.196
(r- θ)	$2.2320_{10^{-5}}$	$2.1270_{10^{-5}}$	1.225	1.312	1.297

Normalization:

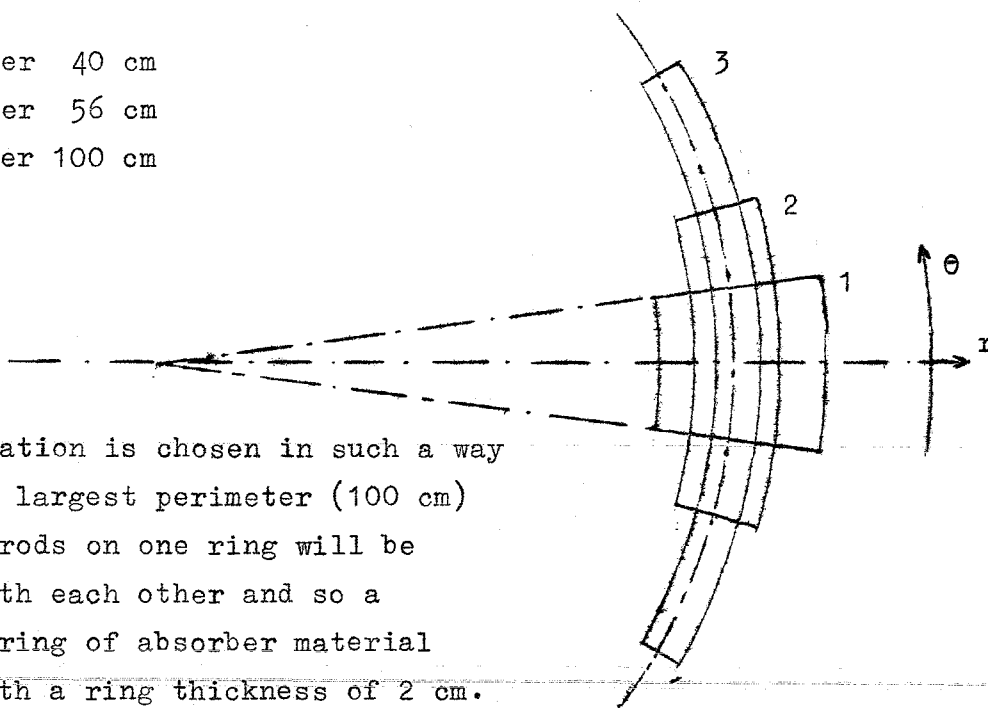
$$\int_{V_{I+II+III}} dV \int_E \Sigma_f \phi dE = 1 \quad \left(\frac{\text{fissions}}{\text{sec}} \right)$$

$$V(\text{zone I}) = 2.63022 \cdot 10^4 \text{ cm}^3$$

$$V(\text{zone II}) = 2.80230 \cdot 10^4 \text{ cm}^3$$

For a constant distance of the rods from the center of the core and a constant cross section of the absorber rod of 95 cm^2 per absorber element the rod perimeter is varied in the $(r - \theta)$ geometry as shown in the next picture:

- 1) perimeter 40 cm
- 2) perimeter 56 cm
- 3) perimeter 100 cm



The configuration is chosen in such a way that for the largest perimeter (100 cm) the control rods on one ring will be connected with each other and so a homogeneous ring of absorber material is formed with a ring thickness of 2 cm.

More-over, the results of the latter configuration can be compared with the results of the one-dimensional calculations.

Table 3.2 shows the reactivity worth as a function of the control rod perimeter. We see that the effect of the rod perimeter is considerable, but not as pronounced as in thermal reactors.

The next point to be considered is the problem of determining the most suitable ring thickness of a homogeneous ring for which the radial fission distribution from a one-dimensional calculation shows the best agreement with the radial fission distribution $p(r)$ of the $(r - \theta)$ calculations in which all control rods are separated. To study this we plotted the one-dimensional radial fission distribution $p = \int \Sigma_f \phi dE$ for three different ring thicknesses (see Fig. 3.1). The fission distribution for the two-dimensional $(r - \theta)$ geometry with inserted rods is given in Fig. 3.2.

It is seen that a homogeneous ring with a thickness of 11 cm gives the best agreement with $(r - \theta)$ calculations, a fact which ensures that the calculations of Chapter 2 are legitimate.

For this reason we decided to perform our two-dimensional (r-z) calculations with rings of 11 cm thickness.

Table 3.2

Reactivity worth of 18 control rods as function of the control rod perimeter in (r - θ) geometry.

perimeter	Δk	
40 cm	0.0622	$R_1 (6) = 45,3$
56 cm	0.0684	$R_2 (12) = \text{boundary}$
77 cm	0.0753	zone I - II
96 cm	0.0748	

3.2 Control Rod Worth for Partially Inserted Rods

For a partially inserted rod along the vertical z-axis we obtain by first order perturbation theory

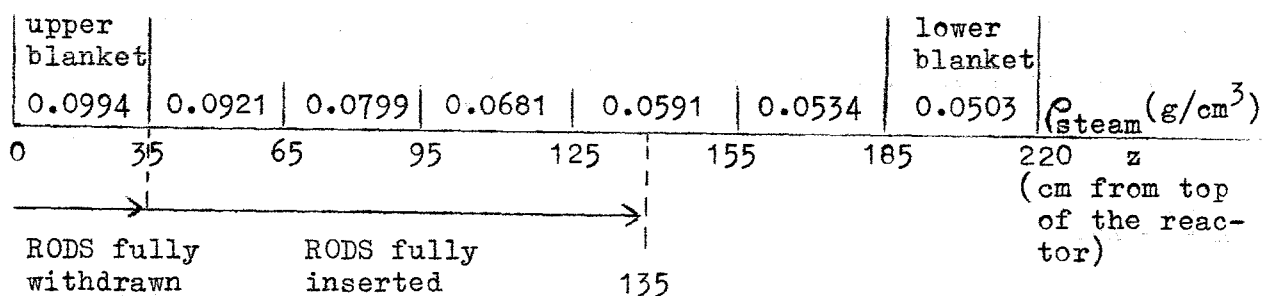
$$\Delta k(z) = \Delta k(H) \frac{\int_0^z \langle \phi^+, \phi \rangle dz}{\int_0^H \langle \phi^+, \phi \rangle dz}$$

in which $\Delta k(z)$ is the reactivity worth of the partially inserted rod to a depth of z cm and $\Delta k(H)$ is the reactivity worth of the fully inserted rod (to a depth of H cm.).

In some one-dimensional axial calculations we determined

$$\frac{\Delta k(z)}{\Delta k(H)} \text{ in two different ways.}$$

In the axial direction the reactor is divided into an upper and a lower blanket and 5 core zones with different steam densities as given in the following sketch:



The sketch shows the geometry for the axial calculations. For the value of y in the core we chose $y=8.72$ and for the radial buckling $B_{\text{rad}}^2 = 2.68 \cdot 10^{-4} \text{ cm}^{-2}$.

For the volume fraction of the absorber material we took 1.6 %/o. The maximum active absorber length H is 100 cm for reasons of reactor construction. The rod will be inserted from the top of the reactor.

With the axial flux distribution of the configuration with fully withdrawn absorber material, we calculated

$$\frac{\int_0^z \langle \phi^+, \phi \rangle dz}{\int_0^H \langle \phi^+, \phi \rangle dz}$$

as a function of the inserted absorber depth z .

In these calculations we approximate $\langle \phi^+, \phi \rangle$ by the product of the fission source $\int_E \nu \Sigma_f \phi dE$ and the neutron fission weight $\int_E \phi^+ / dE$. The results are shown in curve 1 of Fig. 3.3.

In the next step we calculated Δk as a function of the inserted depth by a series of one-dimensional axial calculations for the radially homogenized core. The result of this calculation is curve 2 of Fig. 3.3.

3.3 Optimum Control of the Critical Reactor

3.3.1 Introduction to the Problem

In an operating power reactor we have to insert the absorber rods in such a way that the criticality of the reactor is maintained.

Usually the reactor becomes critical with a few partially inserted absorber rods.

Because the flux distribution in the critical reactor differs greatly from those distributions of the one-dimensional systems with fully inserted control rings, it is evident that the one-dimensional calculations are not the right tool for determining the optimum control rod programming.

The purpose of the calculations we are going to report on now is this:

For a reactor with a fresh fuel loading the excess reactivity must be controlled by inserting some absorber rods in such a way that the reactor becomes just critical and has the most favourable power distribution, i.e. the minimum power factor.

3.3.2 Quantities Kept Constant in the Calculations

In our two-dimensional calculations we locate the 18 control elements on two rings. The inner ring, which is in the inner fission zone, contains 6 control elements. The radius of this ring is fixed at $R_1 = 53.5$ cm, which is between the optimum ring radii determined by the exact calculations and by the synthesis method. (See Chapter 2.3.3). The outer ring contains 12 control elements and is located in the outer fission zone on the boundary of the two fission regions.

In (r-z) calculations the absorber material is smeared in homogeneous rings of 11 cm thickness. Fig. 1.1 gives the dimensions of the cylindrical reactor.

In (r- θ) calculations we chose the control rods with a cross section of 95 cm^2 and a perimeter of 40 cm.

The values of y_I and y_{II} of the two fission zones are chosen in such a way that the reactor in (r- θ) geometry, for a burn-up of 18,000 MWD/tonne (corresponding to the beginning of the reactor cycle) and for fully withdrawn absorber rods gives an excess reactivity of about 1,5 % and that the maximum fission density in the outer fission region (\hat{p}_{II}) is about 10 % above the maximum fission density of the inner fission region (\hat{p}_I).

It was found [1] that with increasing burn-up from 18,000 to

37,000 MWD/tonne, which corresponds to a reactor cycle of 175 days, the ratio \hat{p}_{II}/\hat{p}_I will decrease by about 10 %. Also, if we start up the reactor with 10 % more maximum power density in the outer fission-region, the maximum power density in fission-zone I and II will be about the same at the end of the reactor cycle.

We calculated that for $y_I = 9,74$ and $y_{II} = 7,38$ the above requirements are fulfilled.

For all two-dimensional calculations, we decided to condense the 26 energy groups into a 5-group set. For the condensation spectra we take for each new calculation the 26-group spectra of the corresponding zone obtained from the one-dimensional problem.

The condensation into the 5 groups for all two-dimensional calculations is as follows:

5-group set	group nr.	1	2	3	4	5
26-group set	group nr.	1-5	6-11	12-18	19-24	25-26

3.3.3 Results

In Table 3.3 the numerical results of the two-dimensional (r-z) calculations are given.

N_1 and N_2 are the numbers of B_4C rods which will be inserted in the inner ring and the outer ring. The quantities z_1 and z_2 are the inserted depths of the absorber rods in the core to obtain a critical reactor. The normalization of the values in Table 3.3 is such that $\int_{V_{tot}} dV \int_E \Sigma_f \phi dE = 1$ fissions/sec over the total volume of the reactor. The quantity \hat{p}_{extr} means the estimated maximum fission density at the interface of the first and the second fission zone which may be extrapolated from the fission distribution in the second fission zone. It also represents the maximum fission density between the control rods of the outer ring. (Analogous to the azimuthal fission distribution between the control rods in the (r- θ) calculations.).

The results of the (r- θ) calculations are given in Table 3.4. In the same way as in the one-dimensional calculations the volume integration of the fission density in the (r- θ) geometry is over a core height of 1 cm.

With respect to the fission distribution we calculated for each fission zone and for the total core the maximum fission density, the average fission density and the power factor, which was defined as the ratio of maximum-to-average fission density. To compare the results Table 3.3 contains also some numerical values of the reactor with the absorber rods withdrawn. It can be seen that the reactor with the rods withdrawn gives an excess reactivity of about 1.4 % in the (r-z) geometry and an excess reactivity of 1.6 % in the (r- θ) geometry.

The value $k_{\text{eff}}(z_1, z_2=100 \text{ cm})$ in Table 3.3 means the reactivity of the reactor if all rods of the corresponding configuration are fully inserted (i.e. 100 cm active absorber length in the core).

If we compare the configuration in which 6 control rods are inserted, we see that the configuration with the most favourable fission distribution (low value of the power factor of the total core $\hat{p}_{\text{I+II}} / \bar{p}_{\text{I+II}}$) also has a high value of the control rod worth. It is seen that the configuration of 3 rods inserted in the inner ring and 3 rods inserted in the outer ring has the most favourable value of $\hat{p}_{\text{I+II}} / \bar{p}_{\text{I+II}}$. Next will be the configuration with only 6 rods inserted in the outer ring.

To show the shifting of the spatial fission distributions arising from the insertion of absorber rods into the core we drew the two-dimensional fission distributions for the reactor with the control rods withdrawn and for those two possible control rod configurations which have the best fission distribution for the critical reactor; see Fig. 3.4 to Fig. 3.8.

It is easy to see that the maximum fission density changes to the lower part of the core.

The azimuthal fission distribution between the control rods (especially in the second ring) is expressed in Fig. 3.9 to Fig. 3.11. It is seen that the fission density close to the Al_2O_3 follower rods increases, which is not the case with B_4C absorber rods. This is due to the following effect:

Al_2O_3 is a weak neutron absorber but a good scatterer, so it is expected and verified that around the Al_2O_3 rods the spectrum will be

softer than elsewhere in the core. (Al_2O_3 acts as a moderator.). Because the fission rate increases for lower neutron energy, the fission density near the Al_2O_3 will be higher therefore.

Finally, we plotted in Fig. 3.3 the results $\Delta k(z) / \Delta k(H)$ of the two-dimensional (r-z) calculations. The agreement with the curve from first-order perturbation theory is very good.

Table 3.3

(r-z) Geometry. Critical reactor with partially inserted control rods

N ₁	z ₁ (cm)	N ₂	z ₂ (cm)	k(z, z=100) eff	$\hat{\beta} = \int \Sigma_f \phi dE)_{\max}$			$\int dV \int \Sigma_f \phi dE$			$\frac{\hat{P}_I}{\bar{P}_I}$	$\frac{\hat{P}_{II}}{\bar{P}_{II}}$	$\frac{\hat{P}_{I+II}}{\bar{P}_{I+II}}$	B.R.
					zone I	zone II $\hat{P}(r=102.5)$	zone II \hat{P}_{extr}	zone I	zone II	zone III				
3	74	3	74	0.9908	1.857 ₁₀ ⁻⁷	1.842 ₁₀ ⁻⁷	2.025 ₁₀ ⁻⁷	0.4720	0.4404	0.0629	1.719	1.932	1.808	1.1530
0		6	73	0.9907	2.058 ₁₀ ⁻⁷	1.793 ₁₀ ⁻⁷	1.992 ₁₀ ⁻⁷	0.5030	0.4128	0.0591	1.612	2.030	1.830	1.1525
6	51	6	51	0.9672	1.856 ₁₀ ⁻⁷	1.952 ₁₀ ⁻⁷	2.104 ₁₀ ⁻⁷	0.4640	0.4488	0.0639	1.574	1.971	1.877	1.1510
6	78	0		0.9939	1.674 ₁₀ ⁻⁷	1.948 ₁₀ ⁻⁷	2.150 ₁₀ ⁻⁷	0.4217	0.4849	0.0687	1.569	1.823	1.936	1.1550
0		9	65	0.9841	2.078 ₁₀ ⁻⁷	1.849 ₁₀ ⁻⁷	2.038 ₁₀ ⁻⁷	0.5046	0.4118	0.0590	1.626	2.085	1.850	1.1525
all rods out				k=1.0140	1.730 ₁₀ ⁻⁷	1.791 ₁₀ ⁻⁷	1.960 ₁₀ ⁻⁷	0.4742	0.4417	0.0604	1.435	1.868	1.743	1.142

Normalization: $\int_{V_{\text{tot}}} dV \int_E \Sigma_f \phi dE = 1$ (fissions/sec).

Table 3.4

(r-θ) Geometry. With fully inserted control rods

N ₁	N ₂	k _{eff}	$\hat{\beta} = \int \Sigma_f \phi dE)_{\max}$		$\int dV \int \Sigma_f \phi dE$			$\frac{\hat{P}_I}{\bar{P}_I}$	$\frac{\hat{P}_{II}}{\bar{P}_{II}}$	$\frac{\hat{P}_{I+II}}{\bar{P}_{I+II}}$
			zone I	zone II	zone I	zone II	zone III			
0	0	1.0159	1.959 ₁₀ ⁻⁵	2.270 ₁₀ ⁻⁵	0.4861	0.4570	0.0569	1.060	1.391	1.308
0	6	0.9969	2.394 ₁₀ ⁻⁵	2.320 ₁₀ ⁻⁵	0.5174	0.4268	0.0558	1.217	1.523	1.377
0	9	0.9888	2.662 ₁₀ ⁻⁵	2.558 ₁₀ ⁻⁵	0.5373	0.4082	0.0545	1.303	1.753	1.529
6	0	0.9972	2.030 ₁₀ ⁻⁵	2.430 ₁₀ ⁻⁵	0.4181	0.5149	0.0670	1.277	1.322	1.413

Normalization: $\int_V 2\pi r dr \int_E \Sigma_f \phi dE = 1$ (fissions/sec).

To underline the importance of the fission distribution we calculated, for example, the savings in power generation costs for the two most favourable control rod configurations with respect to the arbitrarily chosen configuration of 6 rods inserted in the inner ring to a depth of 78 cm.

The savings for the configuration of $N_1=3, N_2=3$ to a depth of 74 cm is about DM $11 \cdot 10^6$ a year.

For the configuration with only 6 rods inserted in the outer ring the savings will be about DM $9 \cdot 10^6$ a year.

Finally, it is seen from Table 3.3 that the breeding ratio B.R. varies not so strongly as a function of the method of reactor control. The B.R. is defined here as the ratio of the integral capture rate in the fertile material to the capture and fission rate in the fissile material. (The integration is over the total volume of the reactor).

3.3.4 Discussion

~~We have to be careful to compare these results of the two-dimensional calculations for the critical reactor with the results of the one-dimensional calculations because the two-dimensional calculations have two different starting points compared to the one-dimensional calculations. These differences will be explained below:~~

To simulate the power distribution corresponding to the condition of lowest burn-up, which occurs after reloading of fuel elements, the fuel enrichments in the core were chosen in such a way for the two-dimensional calculations as to make the maximum power density in zone II 10 % higher than the maximum power density in zone I. The result is that the ratio of the fuel enrichment in zone II to that in zone I is higher than the ratio used in the one-dimensional calculations. So, the power factor for the unperturbed reactor is higher for the two-dimensional geometry. The next point is connected with the fact that in the two-dimensional calculations of this chapter we always used the configuration of 6 control elements on a inner ring and 12 control elements at the interface of zone I-zone II. In the one-dimensional calculations, however, only for a few cases a ring of 12 control elements was present at the interface of zone I-zone II. Exchanging fuel rods by either control or

follower rods at this position greatly influences the power distribution. Because the maximum power density occurs at the interface zone I-zone II in most cases the power factor is influenced also. So, care must be taken in the comparison of the two-dimensional results of this chapter with the one-dimensional results of the preceding chapter.

The (r-z) and (r- θ) calculations are very useful to show the tendencies of the reactivity worth and fission distribution. To determine more realistic absolute values of the shutdown reactivity and control rod worth, proper three-dimensional calculations will be preferable.

4. Conclusion

As we have seen before, this investigation had two purposes. The conclusion of Chapter 2 is that the optimum location for maximum shutdown reactivity of a single or two rings of absorber elements can be determined very well by one-dimensional calculations.

For the cases studied it was further seen that the configuration with maximum control rod worth for the absorber rings also has a favourable fission distribution.

The two-dimensional ($r-\theta$) calculations showed that we have to perform the calculations in a better geometric arrangement to determine more accurately the absolute values of the control rod worths.

The examples of Chapter 3 showed that it is desirable to determine that special location and insertion depth of the shim rods for which it is possible to maintain the reactor critical with the most favourable fission distribution.

The ($r-z$) calculations show (Table 3.3) that the insertion of three rods in the inner ring and three rods in the outer ring results in the best fission distribution, but the difference to the case of six rods inserted in the outer ring is not so pronounced.

Acknowledgement

The author would like to thank Prof. K. Wirtz for the opportunity to complete this study at the Institute of Neutron Physics and Reactor Engineering.

In particular, I am grateful to Dr. E. Kiefhaber for the many valuable discussions and advice in all phases of the investigation.

I would like to thank everybody at Karlsruhe who helped making my stay in Germany instructive and rewarding.

References

- [1] A. Müller et al. Referenzstudie für den 1000 MWe dampfgekühlten schnellen Brutreaktor (D-1), KFK-392, August 1966
- [2] H. Bachmann et al. The Karlsruhe Nuclear Code System NUSYS.
(not published)
- [3] L.P. Abagjan et al. Gruppen Konstanten schneller und intermediärer Neutronen für die Berechnung von Kernreaktoren.
KFK-tr-144 (1965)

Fig. 2.1 Volume integrated capture rate of B^{10} as function of the neutron energy for the unperturbed reactor

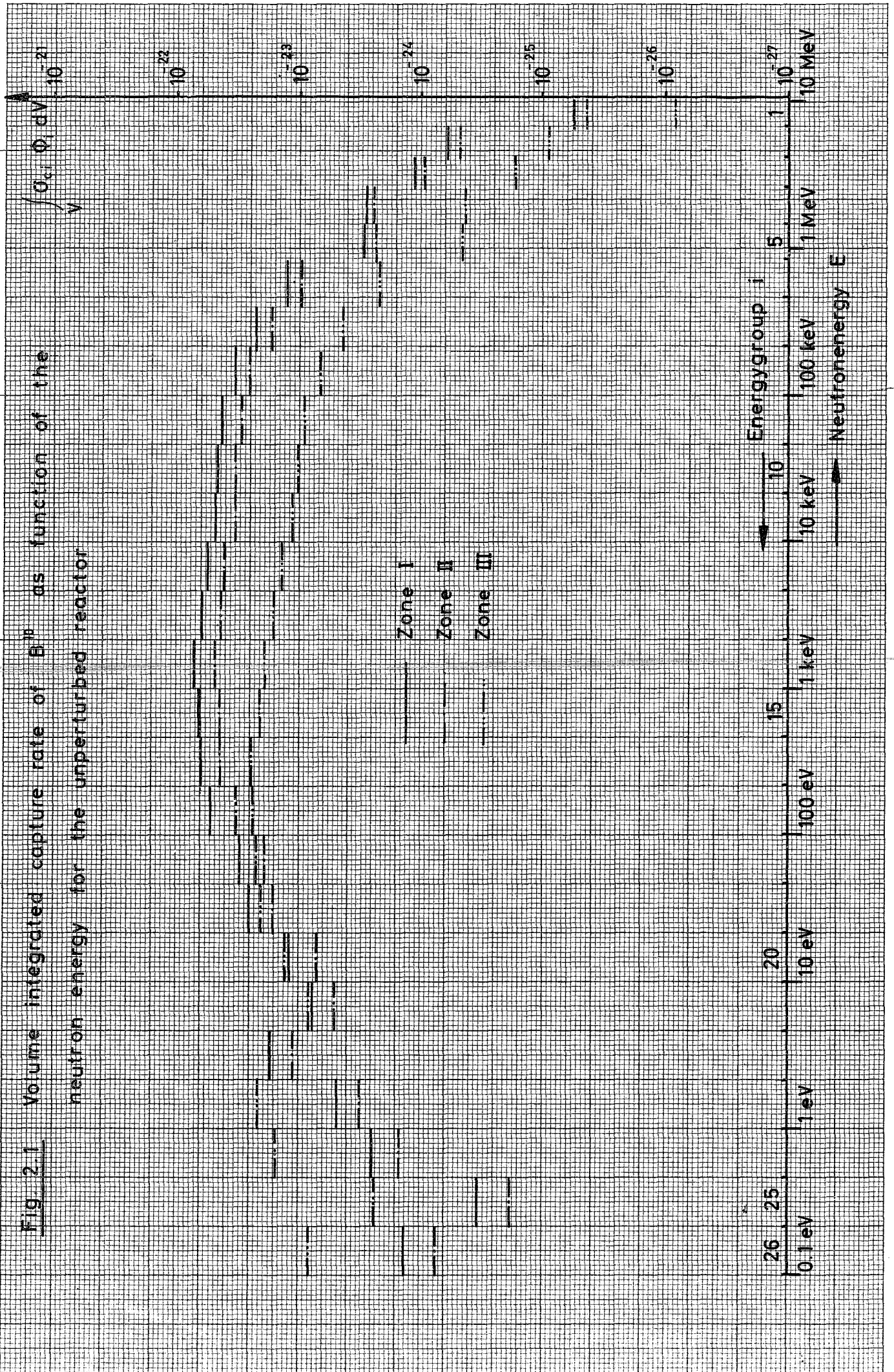


Fig. 2.2 Reactivity worth per control element as function of the radius of one cylindrical absorber ring

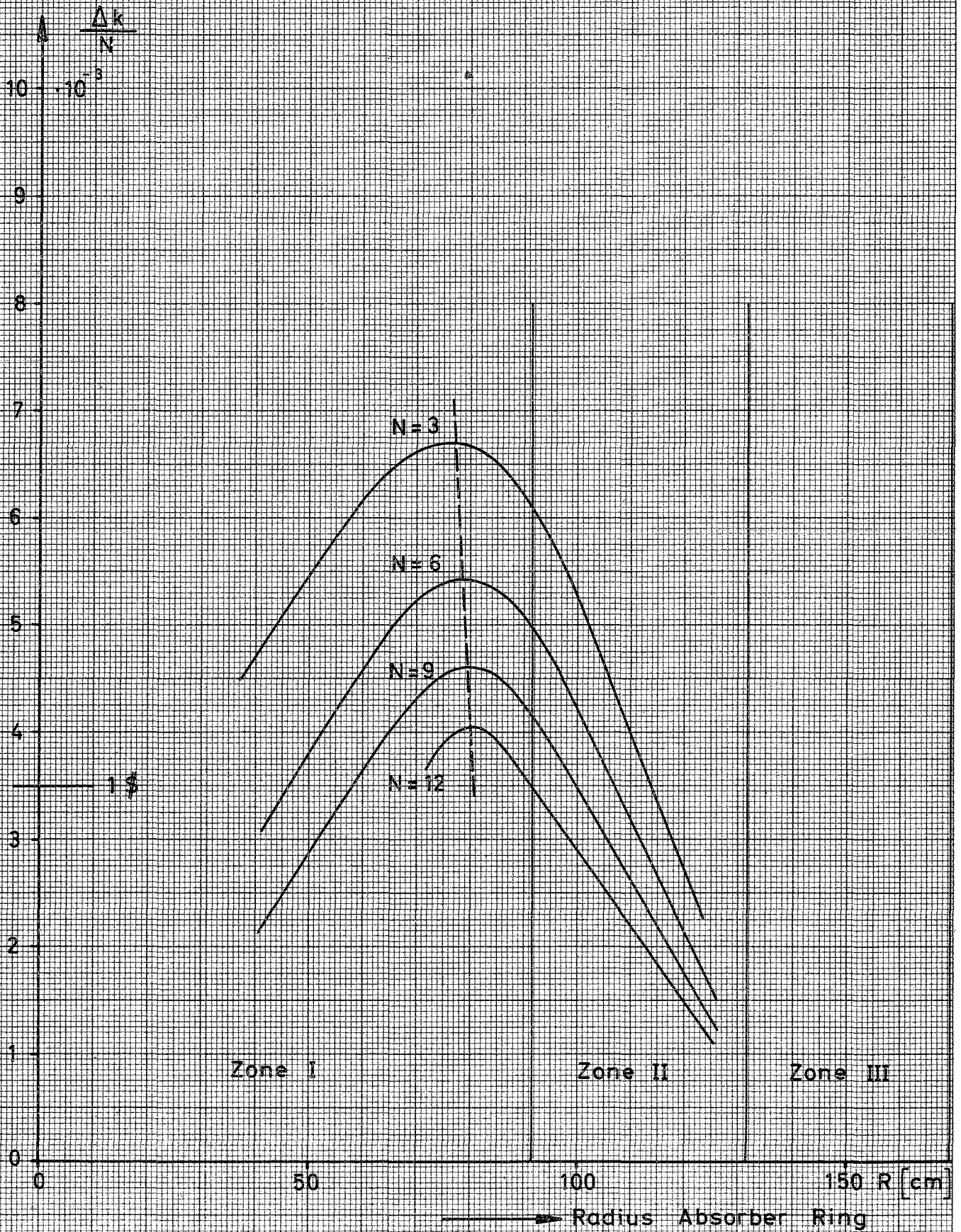


Fig. 2.3. Radial dependence of the capture rate of B^{10} for the reactor with one absorber ring of radius $R = 43.0$ cm

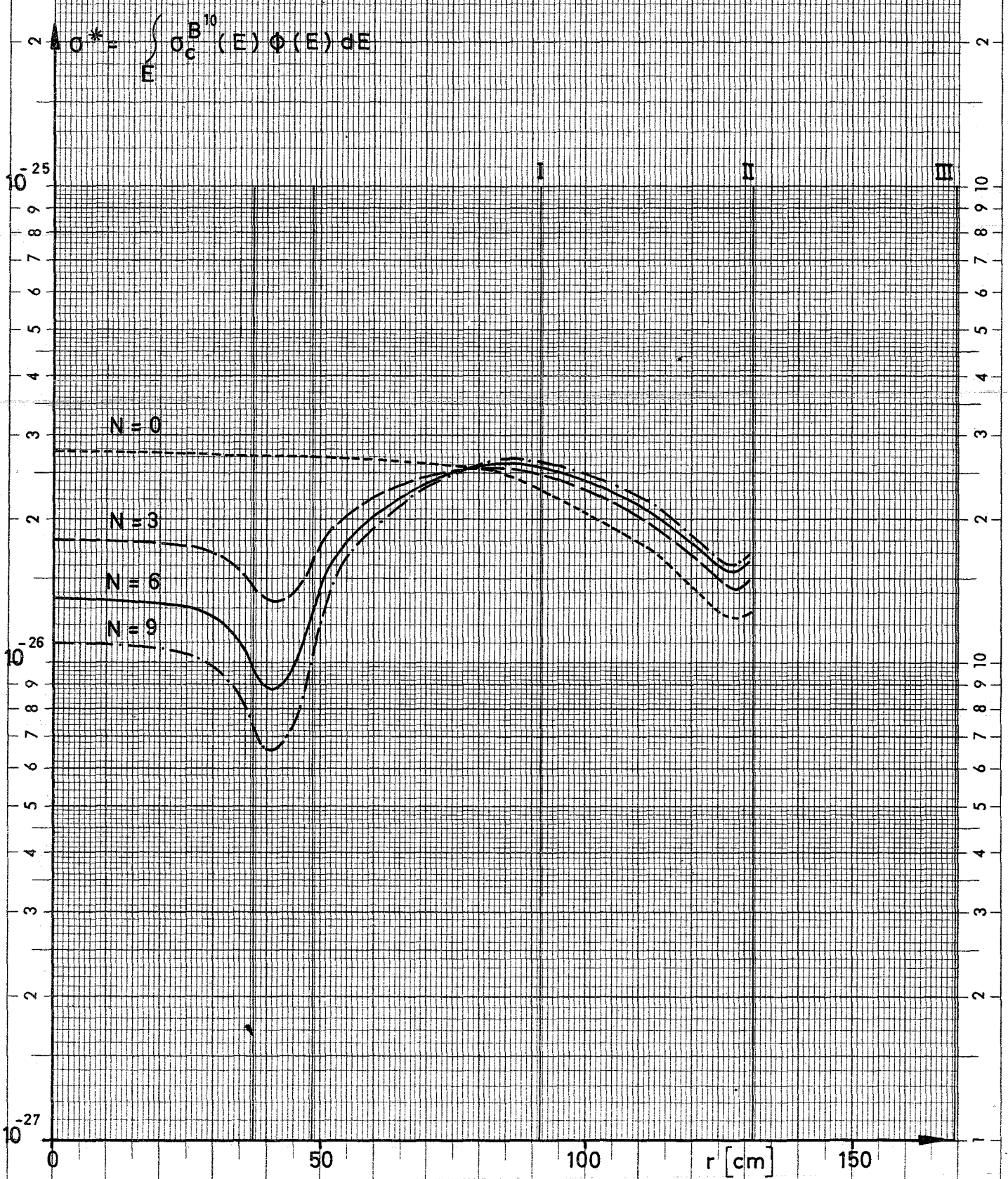


Fig. 2.4 Radial dependence of the capture rate of B^{10} for the reactor with one absorber ring of radius $R = 97.0$ cm

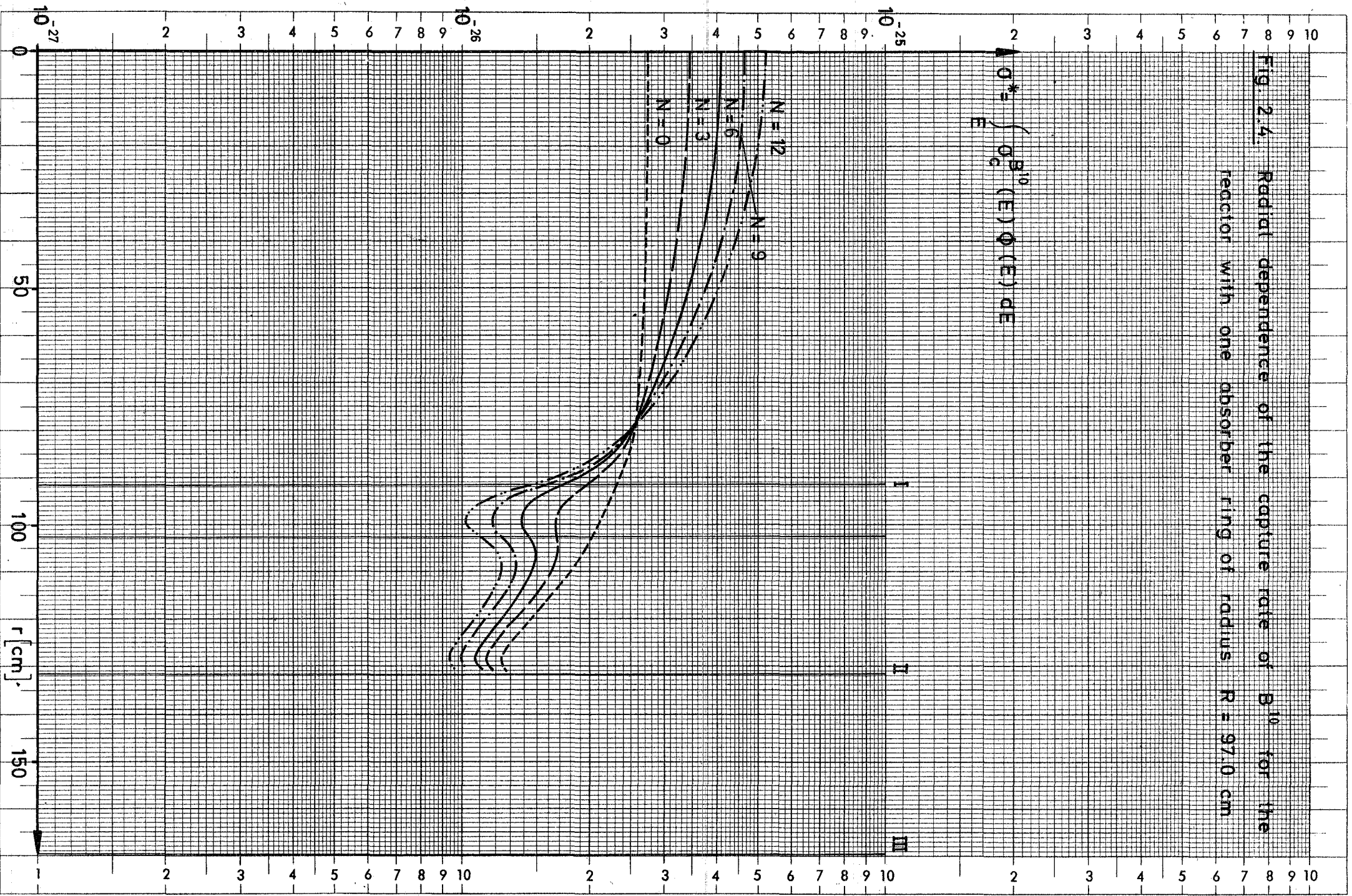
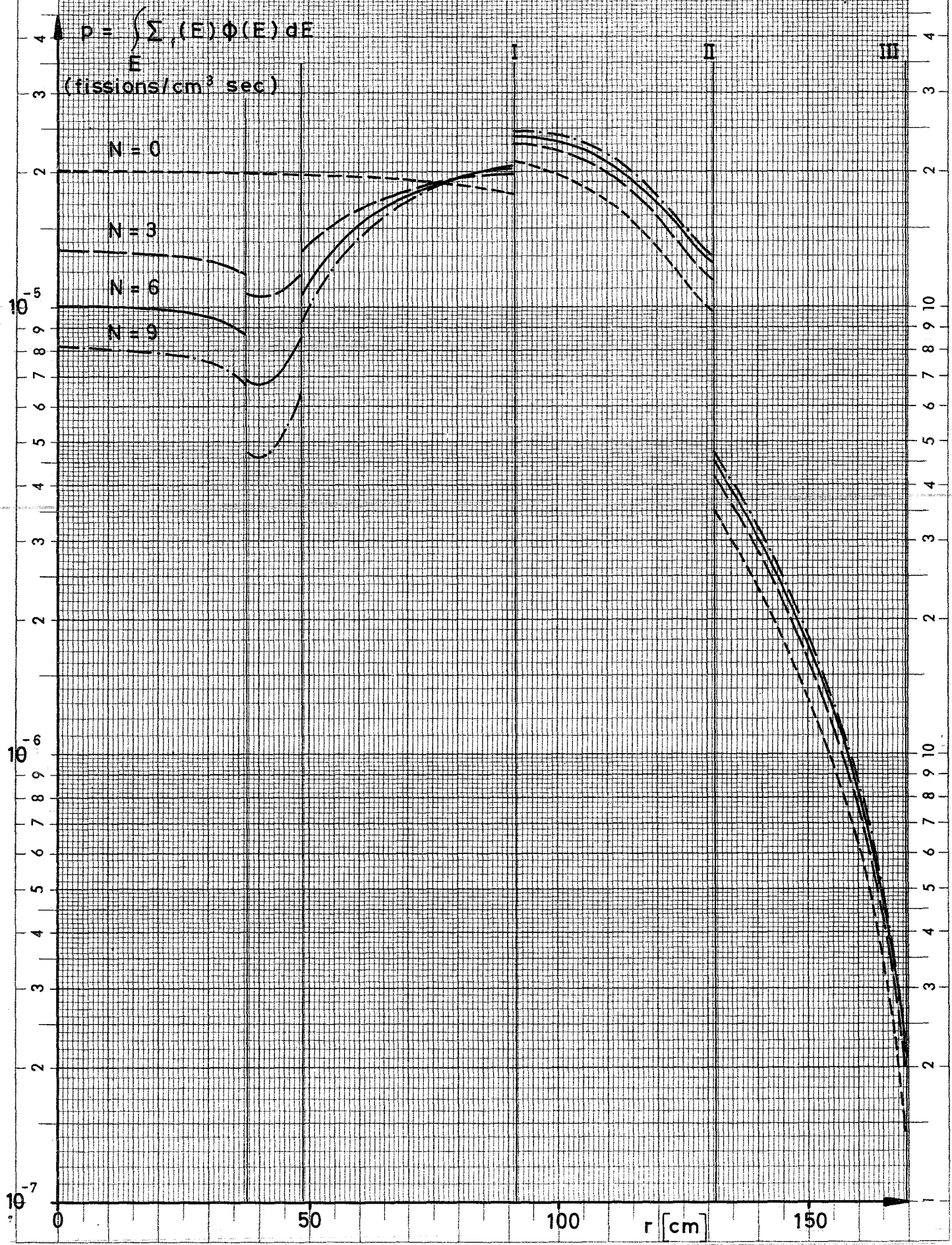


Fig. 2.5. Radial dependence of the fission rate for the reactor with one absorber ring of radius $R = 43.0$ cm



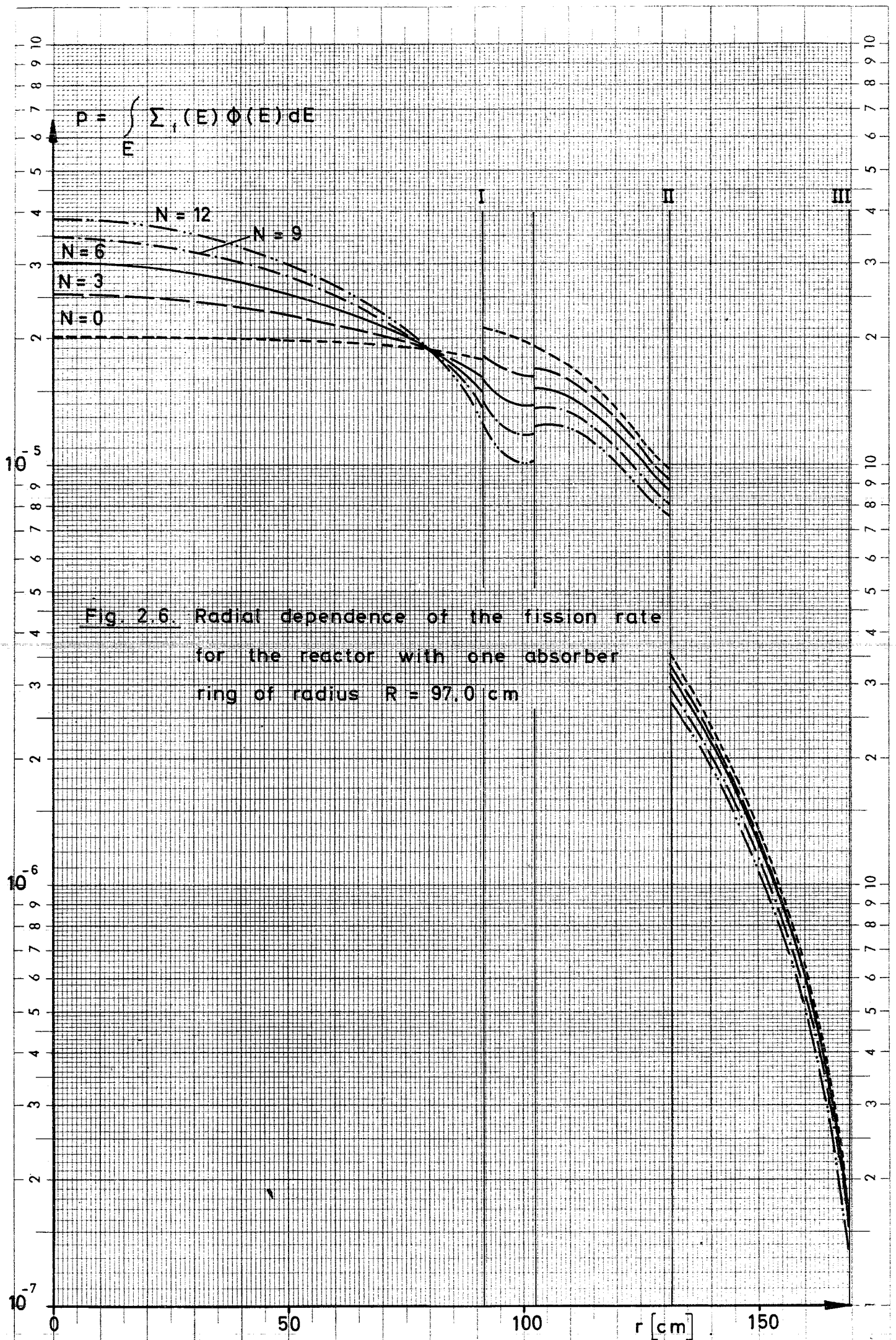


Fig. 2.6. Radial dependence of the fission rate for the reactor with one absorber ring of radius $R = 97.0$ cm

Fig 2.7. Radial dependence of the capture rate of B^{10} for the reactor with two absorber rings

$$\sigma^* = \int_E \sigma_c^{B^{10}}(E) \Phi(E) dE$$

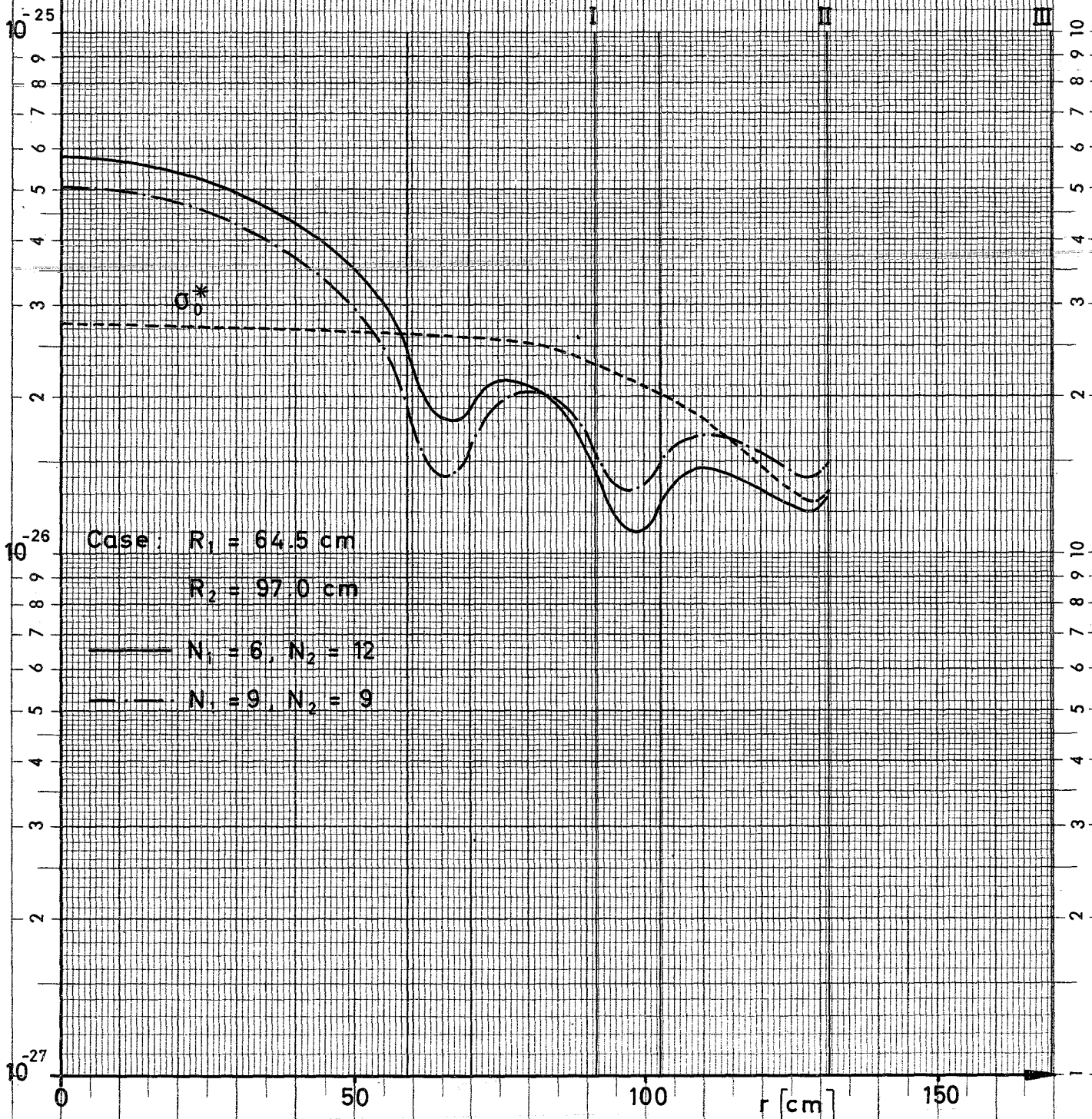


Fig. 2.9. Total reactivity worth for the reactor configuration of two cylindrical control rings as function of the radius of the inner absorber ring

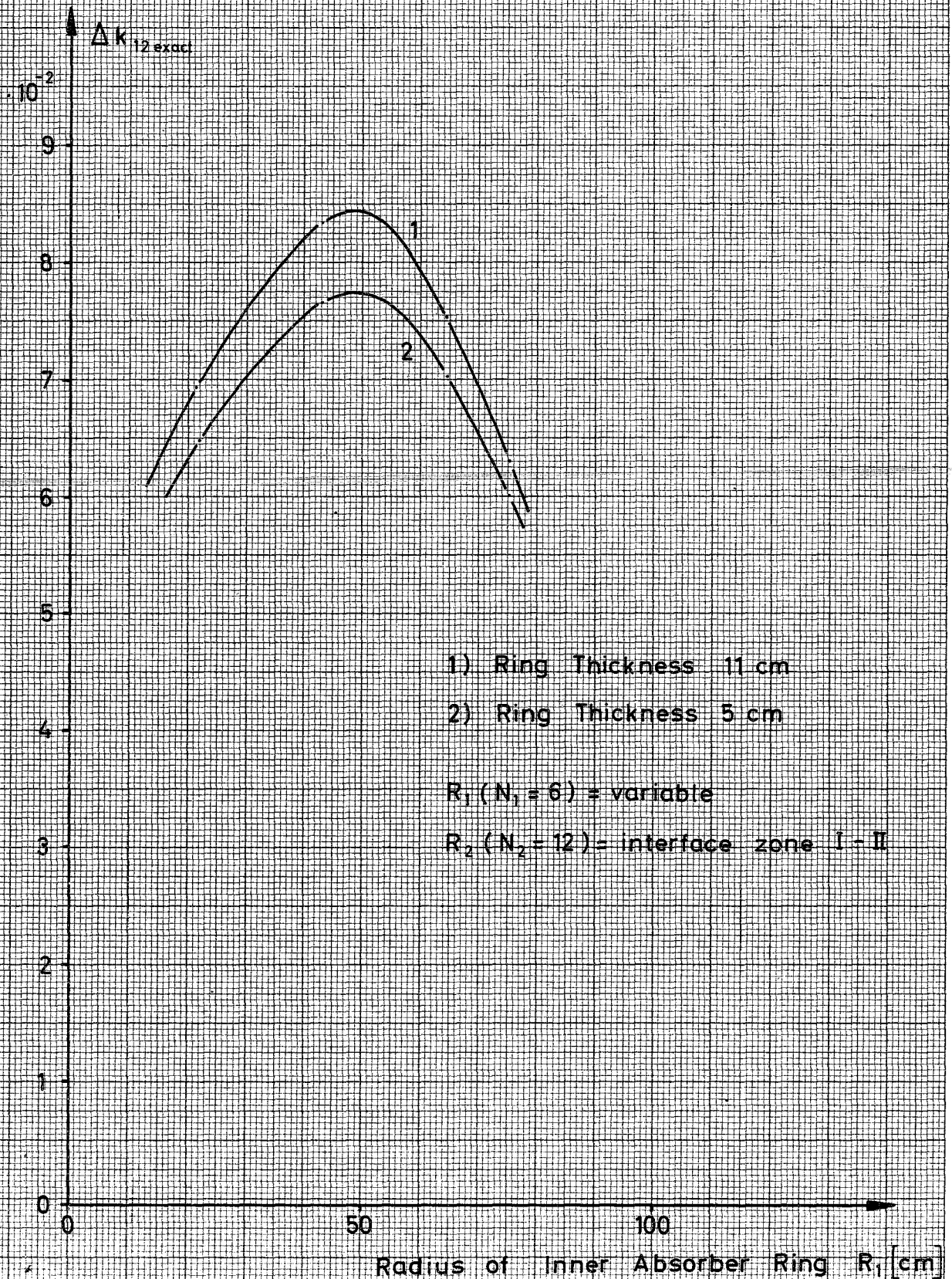


Fig. 2.10. Comparison of the capture rate of B^{10} from direct two-ring results and single ring calculations

Case: $R_1 (N_1 = 6) = 43.0 \text{ cm}$

$R_2 (N_2 = 12) = 97.0 \text{ cm}$

$$\text{---} \frac{\sigma_{12}^*}{\sigma_0^*}$$

$$\text{- - -} \frac{\sigma_1^*}{\sigma_0^*} \cdot \frac{\sigma_2^*}{\sigma_0^*}$$

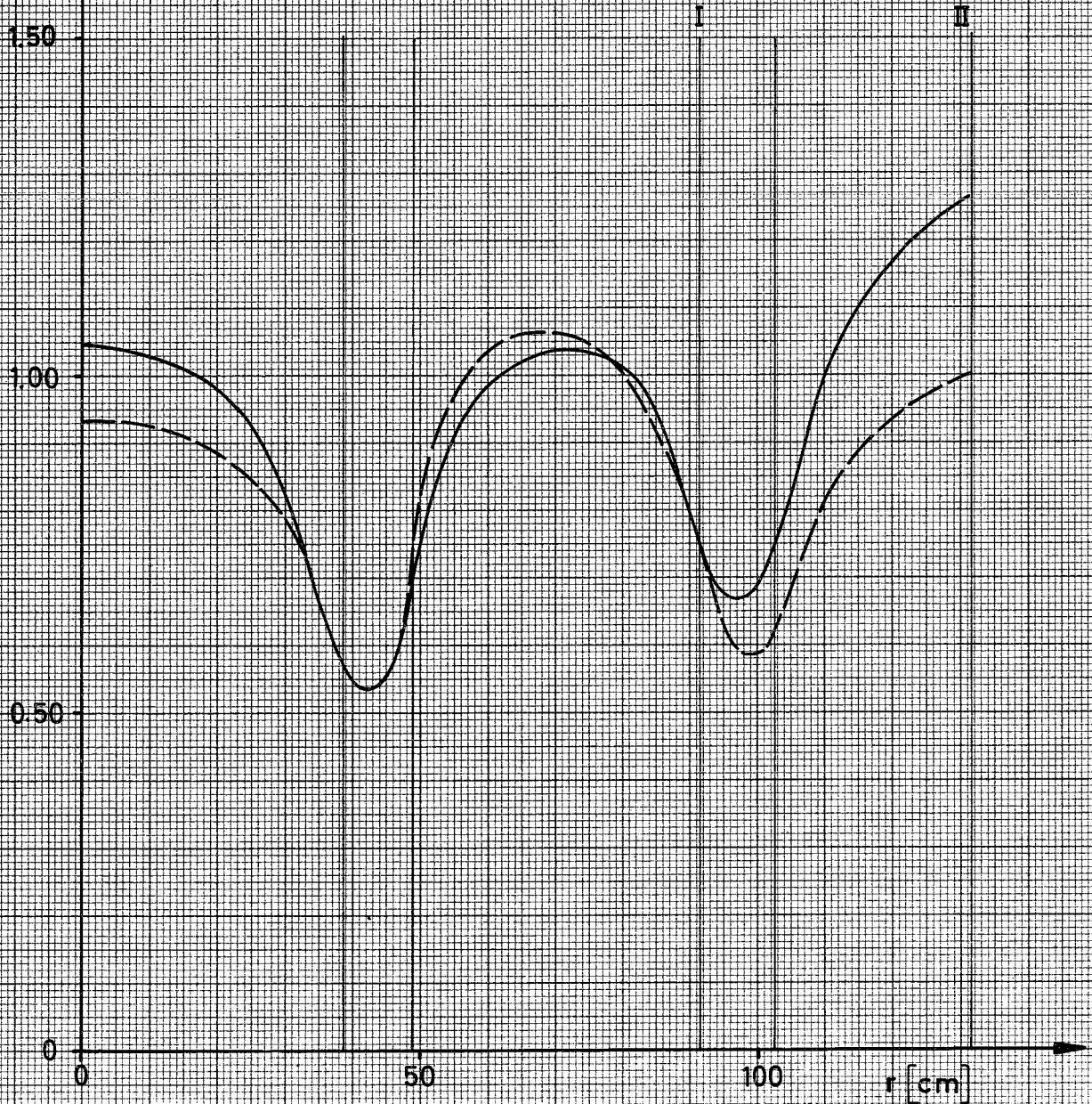


Fig. 2.11. Comparison of the neutron fission weight from direct two-ring results and single ring calculations

Case: $R_1 (N_1 = 6) = 43.0 \text{ cm}$

$R_2 (N_2 = 12) = 97.0 \text{ cm}$

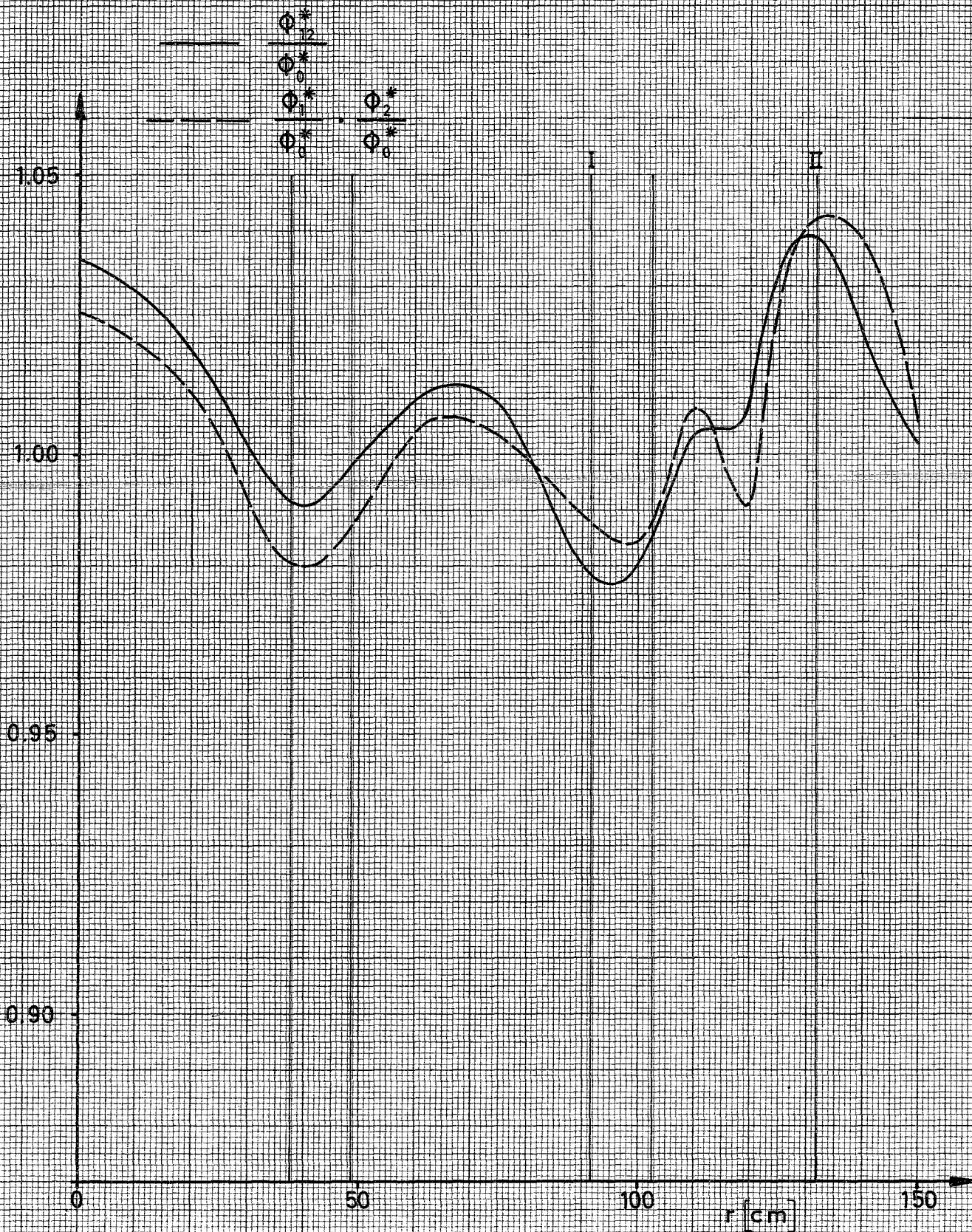


Fig. 2.12. Calculated reactivity worth as function of the radius of the inner absorber ring

Case: $N_1 = 6$

$N_2 = 12$

$\cdot 10^{-2}$

Δk_{12}

8

7

6

5

4

b

c

a

d

a) $R_2 = 75.25$ cm

b) $R_2 = 86.0$ cm

c) $R_2 = 97.0$ cm

d) $R_2 = 111.5$ cm

$$\Delta k_{12} = \frac{\phi_2^*(R_1)}{\phi_0^*(R_1)} \frac{\sigma_2^*(R_1)}{\sigma_0^*(R_1)} \Delta k_1 + \frac{\phi_1^*(R_2)}{\phi_0^*(R_2)} \frac{\sigma_1^*(R_2)}{\sigma_0^*(R_2)} \Delta k_2$$

Radius for Inner Absorber Ring R_1 [cm]

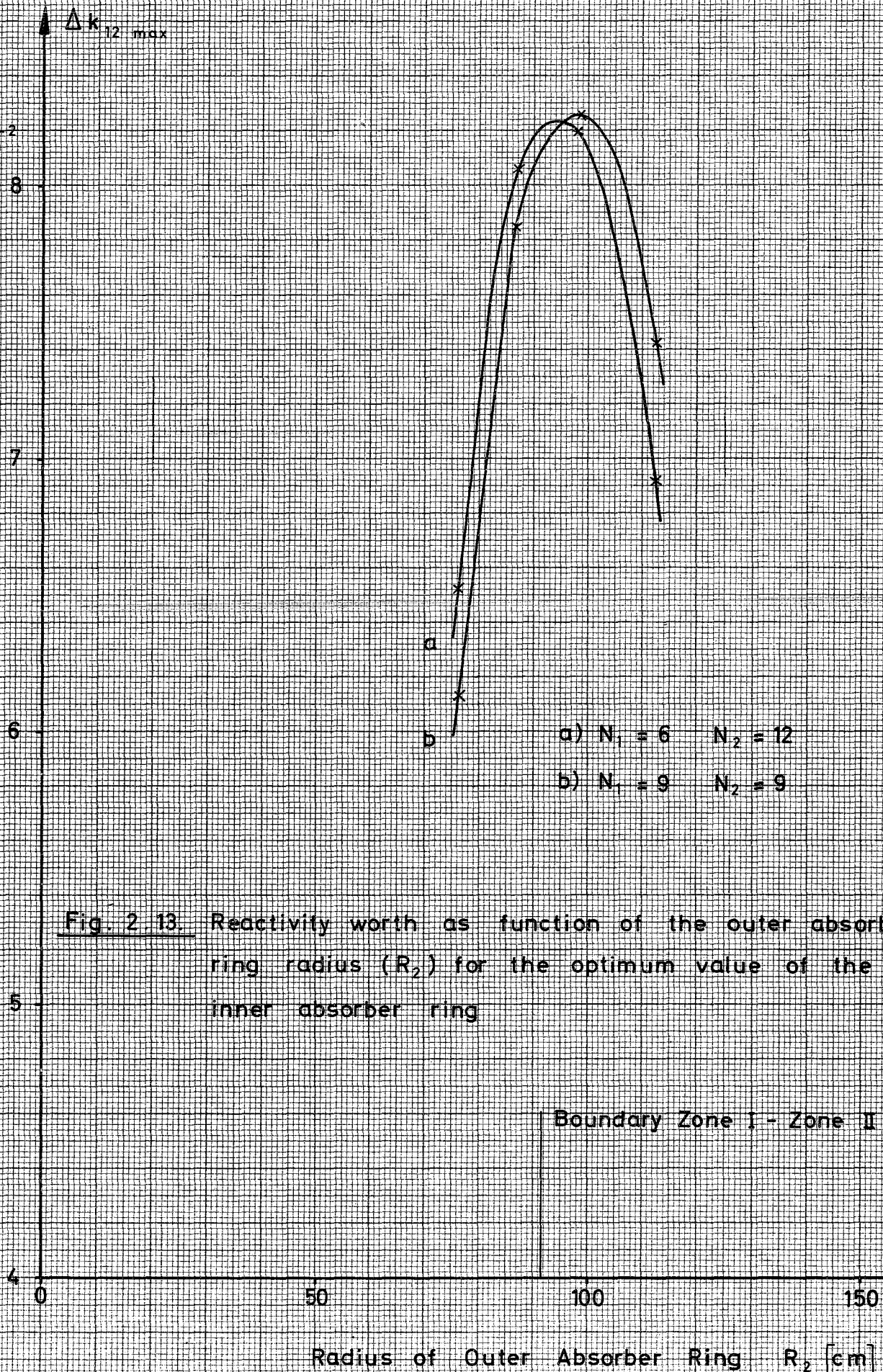


Fig. 2 13. Reactivity worth as function of the outer absorber ring radius (R_2) for the optimum value of the inner absorber ring

Boundary Zone I - Zone II

Radius of Outer Absorber Ring R_2 [cm]

Fig. 2.14. Optimum radius of the inner absorber ring as function of the location of the outer absorber ring

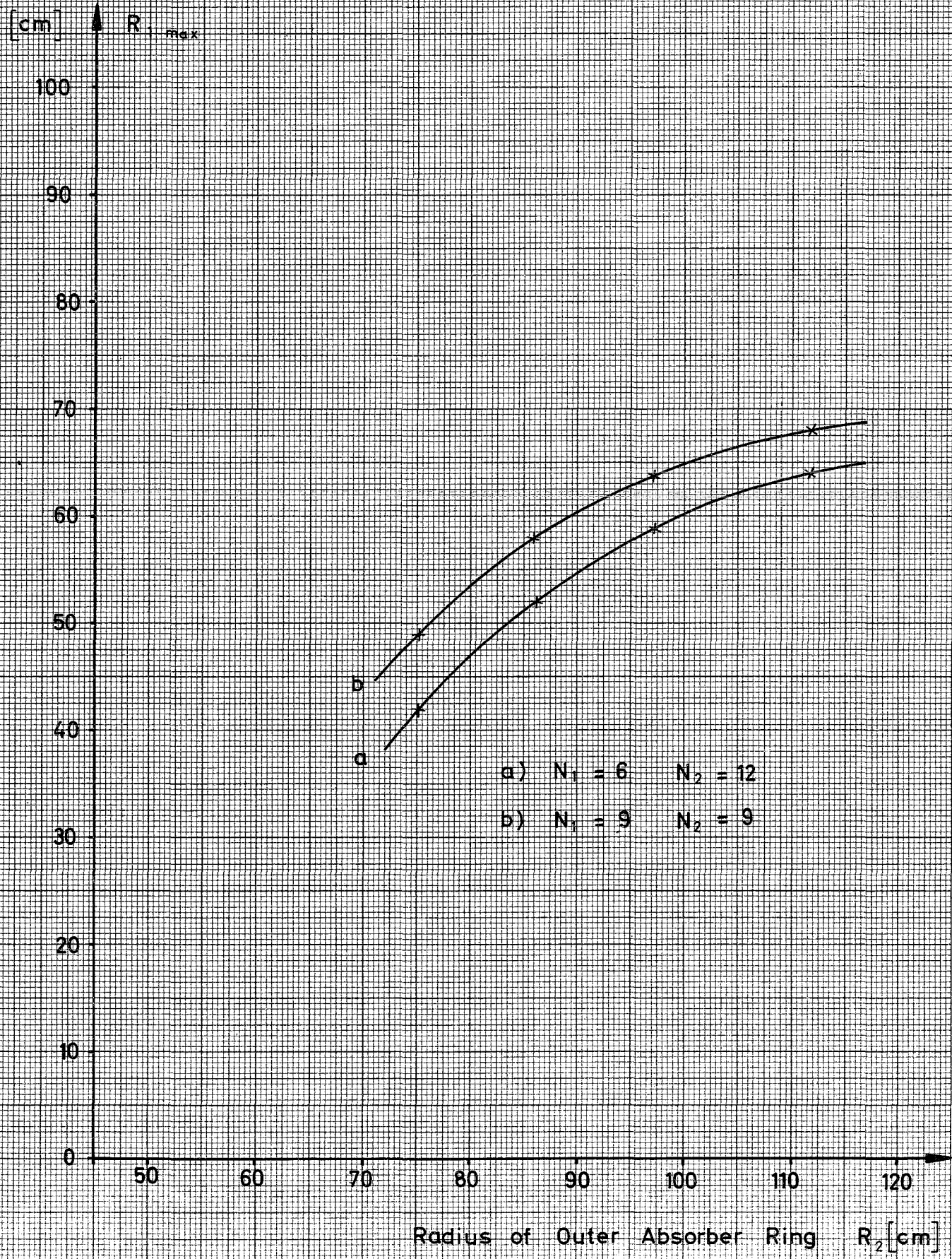


Fig. 3.1. One dimensional radial fission distribution
for three different ring thicknesses

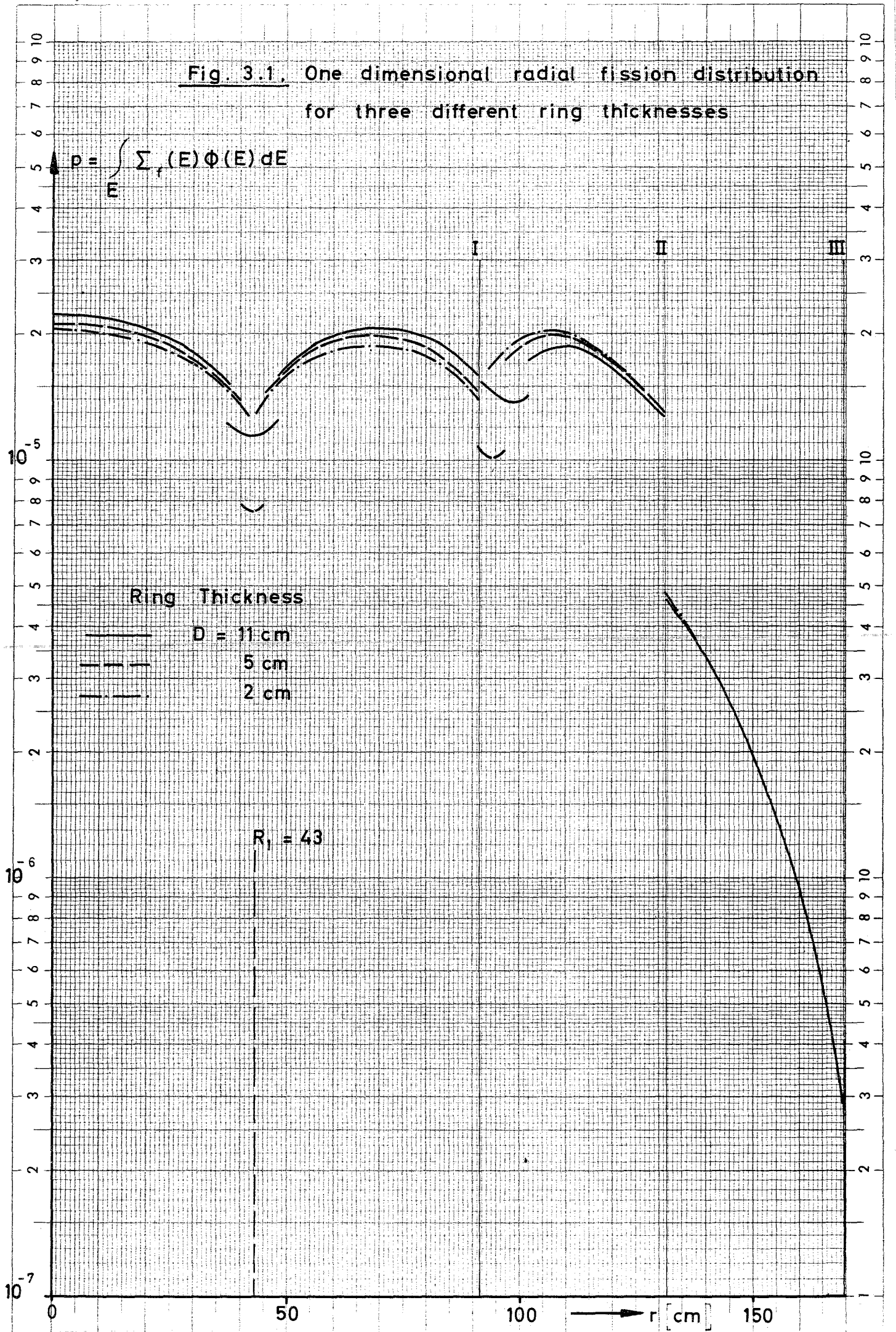


Fig. 3.2. Radial fission distribution in two-dimensional ($r-\theta$) geometry for the reactor with all control rods inserted

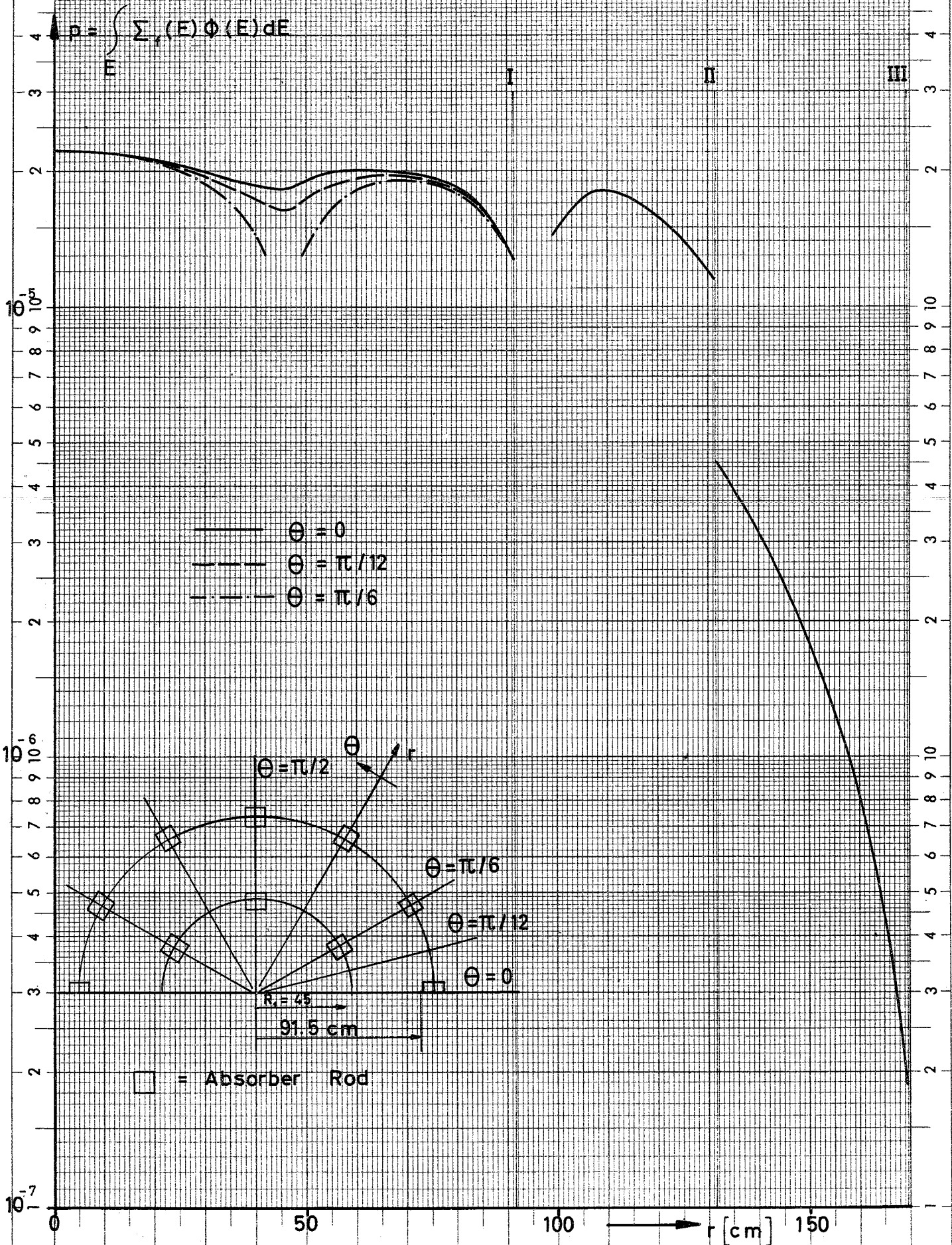


Fig. 3.3. Reactivity worth as function of the inserted absorber depth

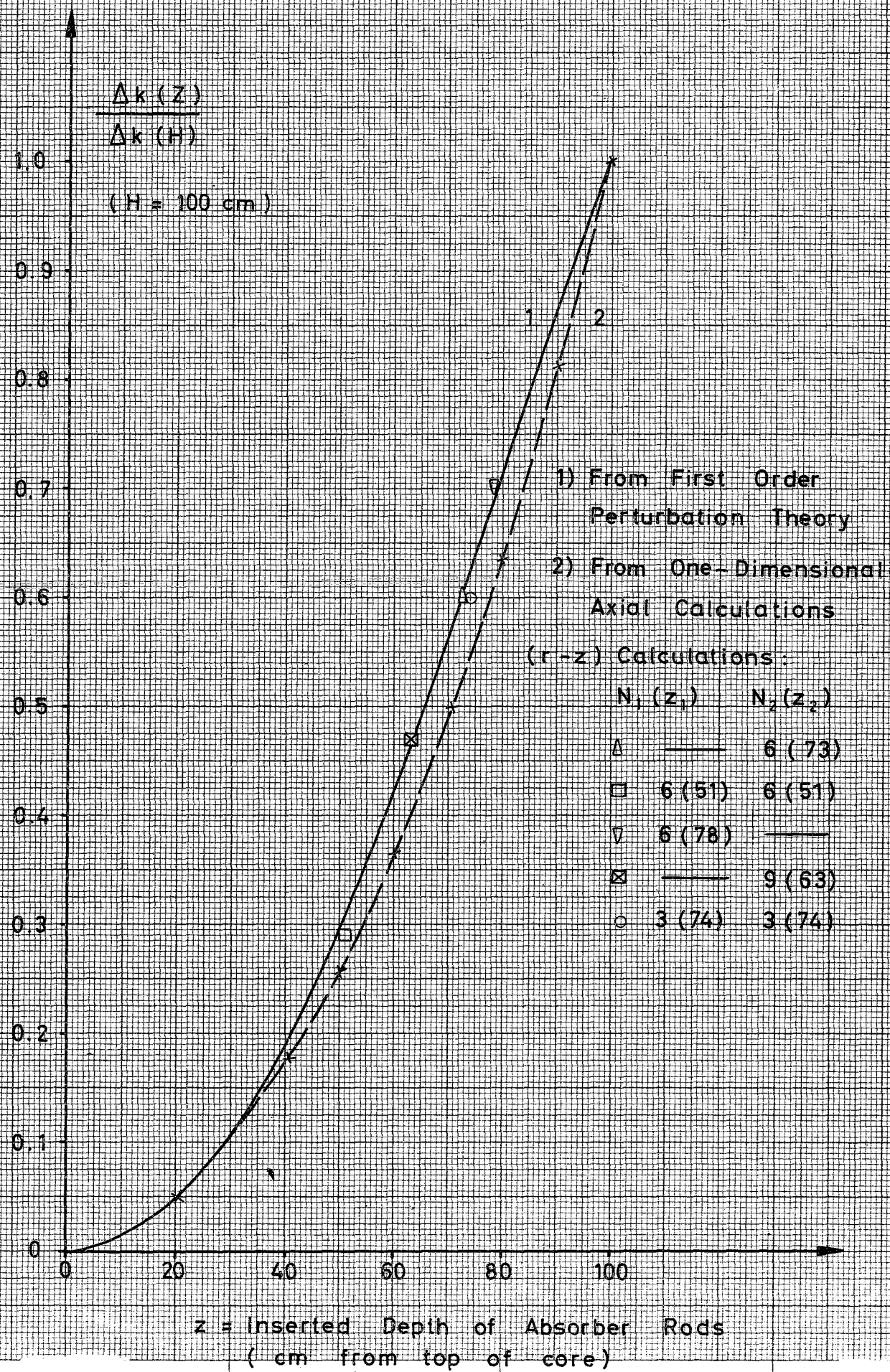


Fig. 3.4. Radial fission distribution in (r-z) geometry for the critical reactor with 6 control rods inserted in the outer ring to a depth of 73 cm

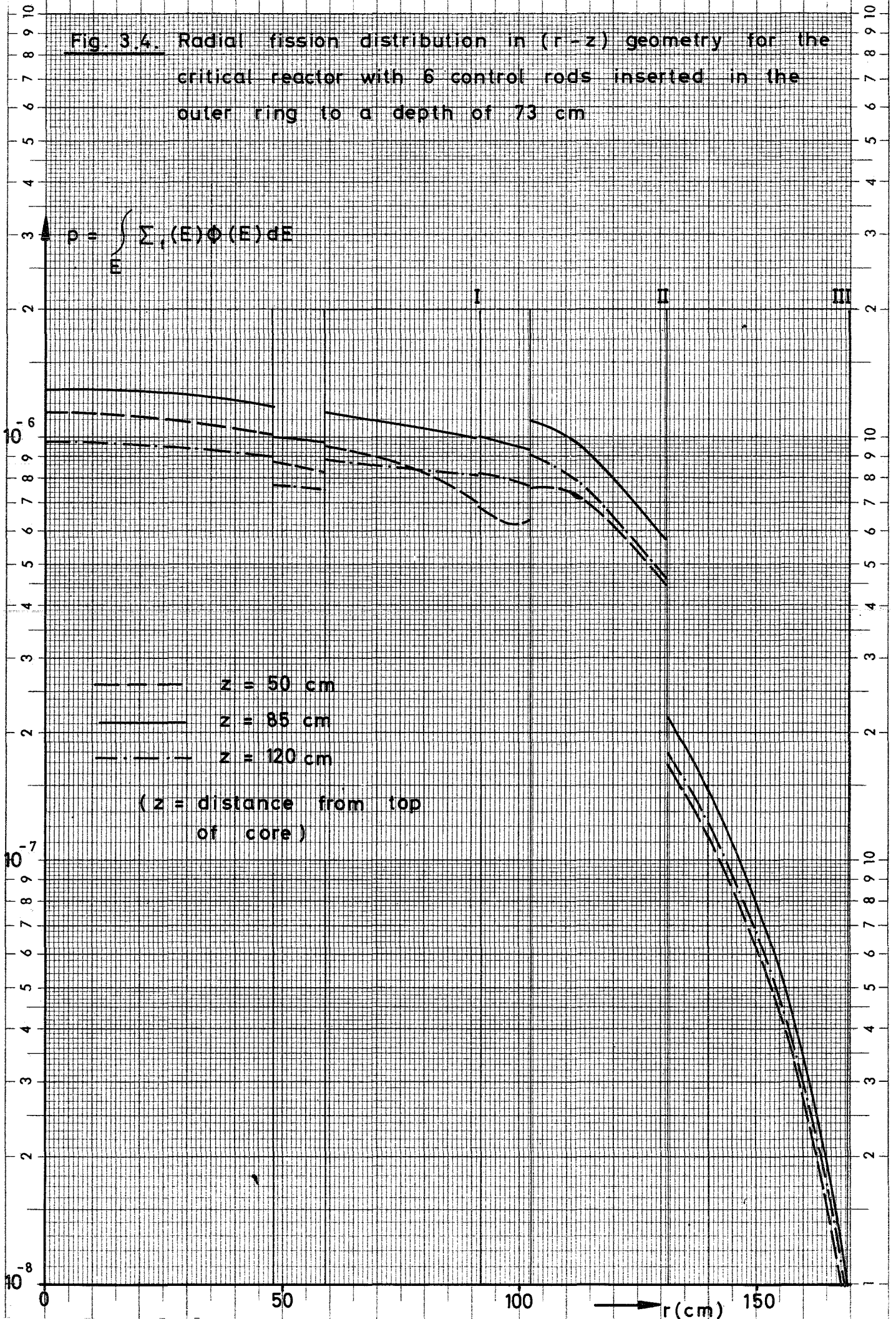


Fig. 3.5. Radial fission distribution in $(r-\theta)$ geometry for 6 rods inserted in the outer ring

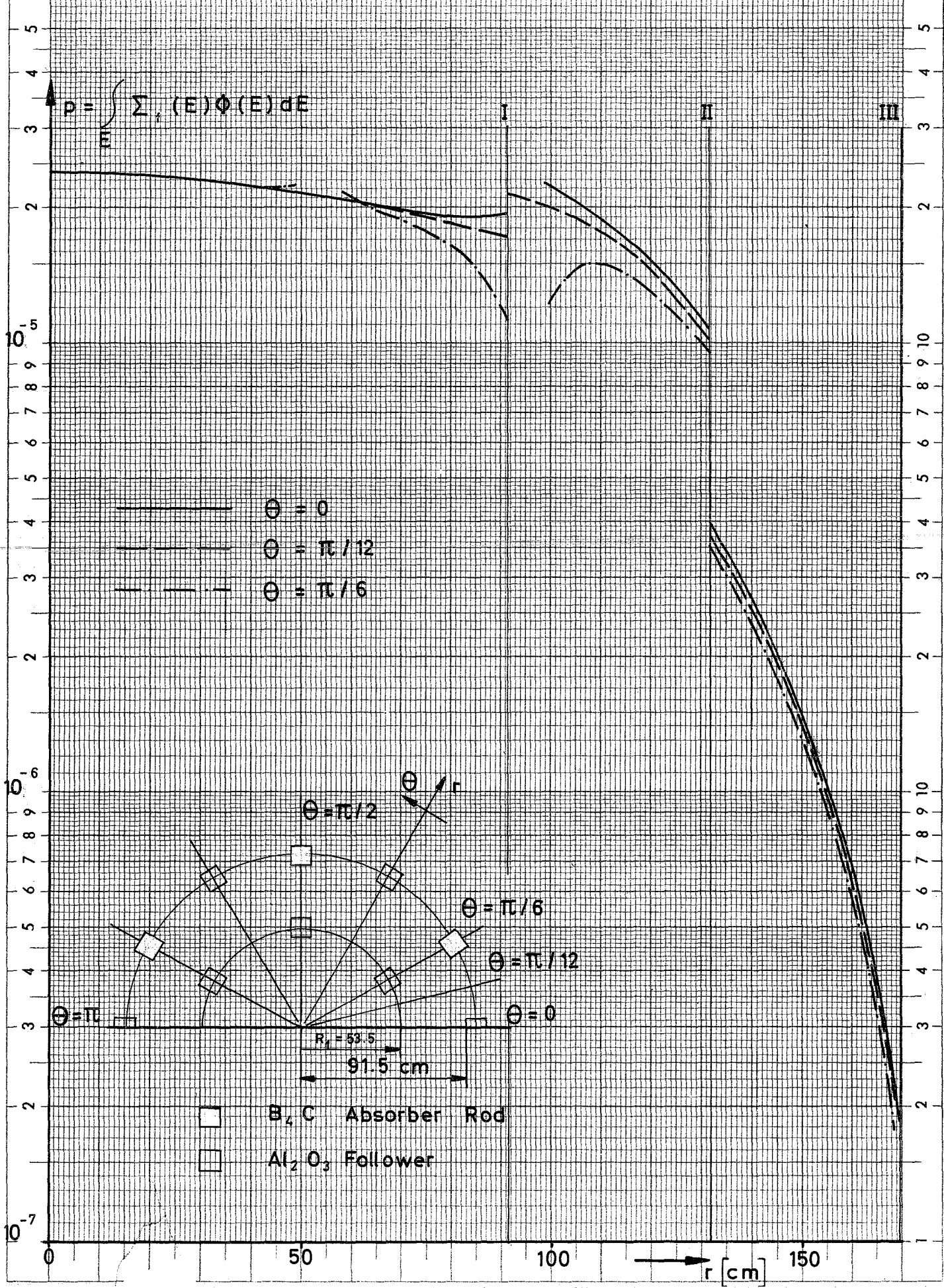


Fig. 3.6. Two-dimensional fission distribution for the reactor in (r-z) geometry with all absorber rods withdrawn

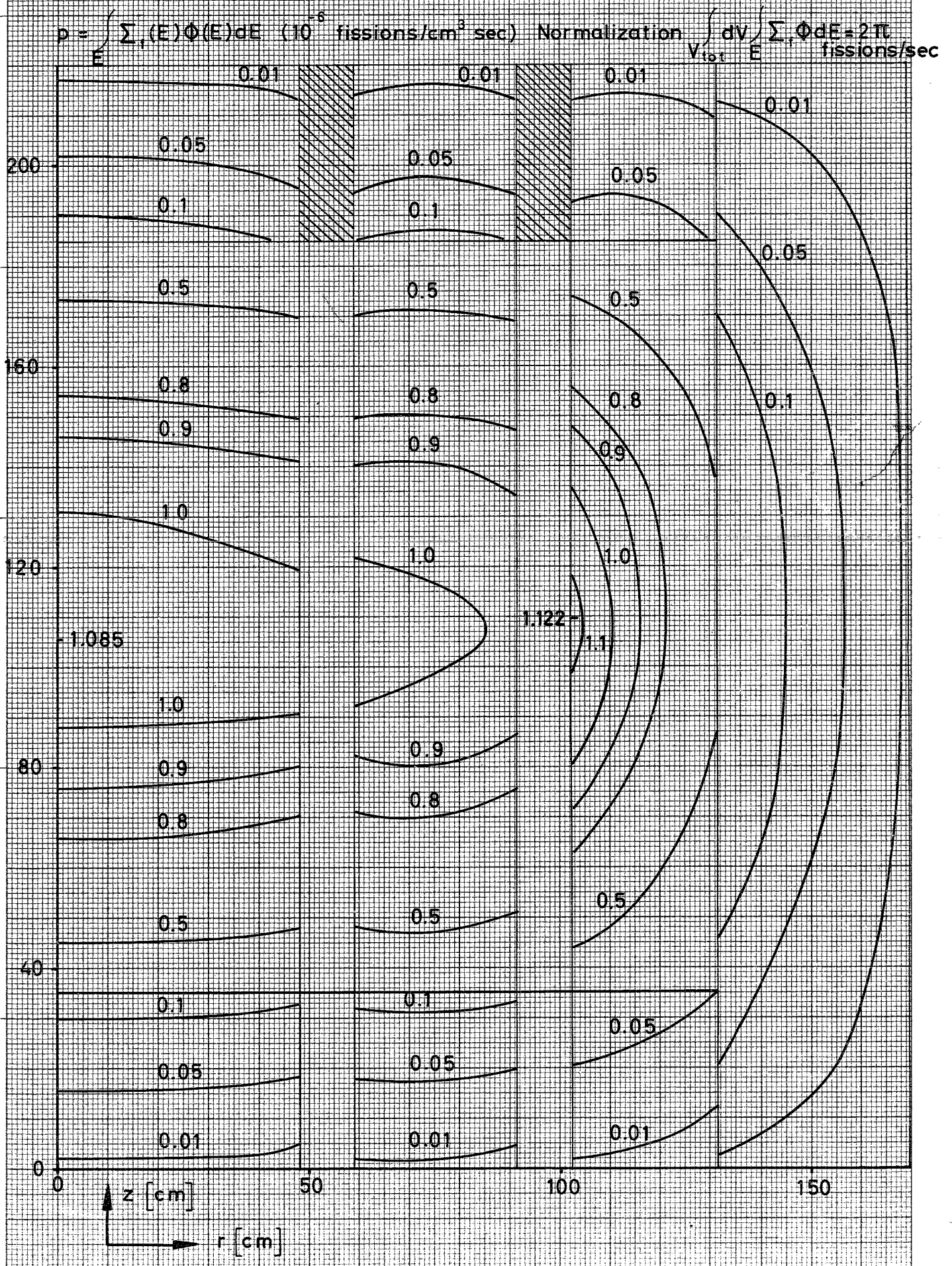


Fig. 3.7. Two-dimensional fission distribution for the critical reactor in (r-z) geometry

Case: $N_1 = 0$, $N_2(z_2 = 73) = 6$

$$\rho = \int \Sigma_f(E) \Phi(E) dE \quad (10^{-6} \text{ fissions/cm}^3 \text{ sec}) \quad \text{Normalization} \quad \int_{V_{\text{tot}}} \int \Phi dE = 2\pi \int \text{fissions/sec}$$

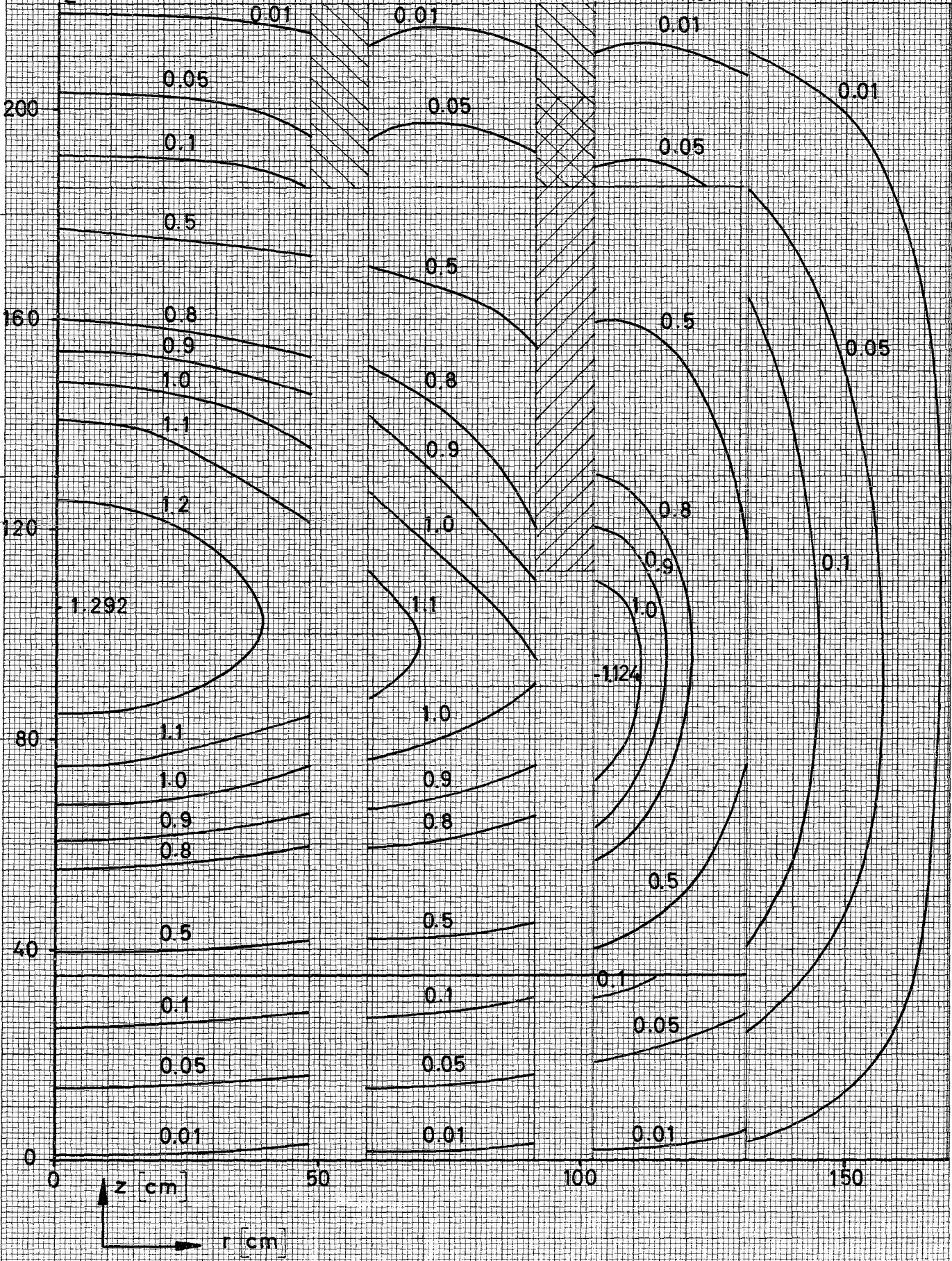


Fig 3.8. Two-dimensional fission distribution for the critical reactor in (r-z) geometry.

Case: $N_1(z_1 = 74) = 3$, $N_2(z_2 = 74) = 3$

$$\rho = \int_E \sum_i (E) \Phi(E) dE \quad (10^6 \text{ fissions/cm}^3\text{sec}) \quad \text{Normalization} \quad \int_{V_{\text{tot}}} \sum_i \Phi dE = 2\pi \int \text{fissions/sec}$$

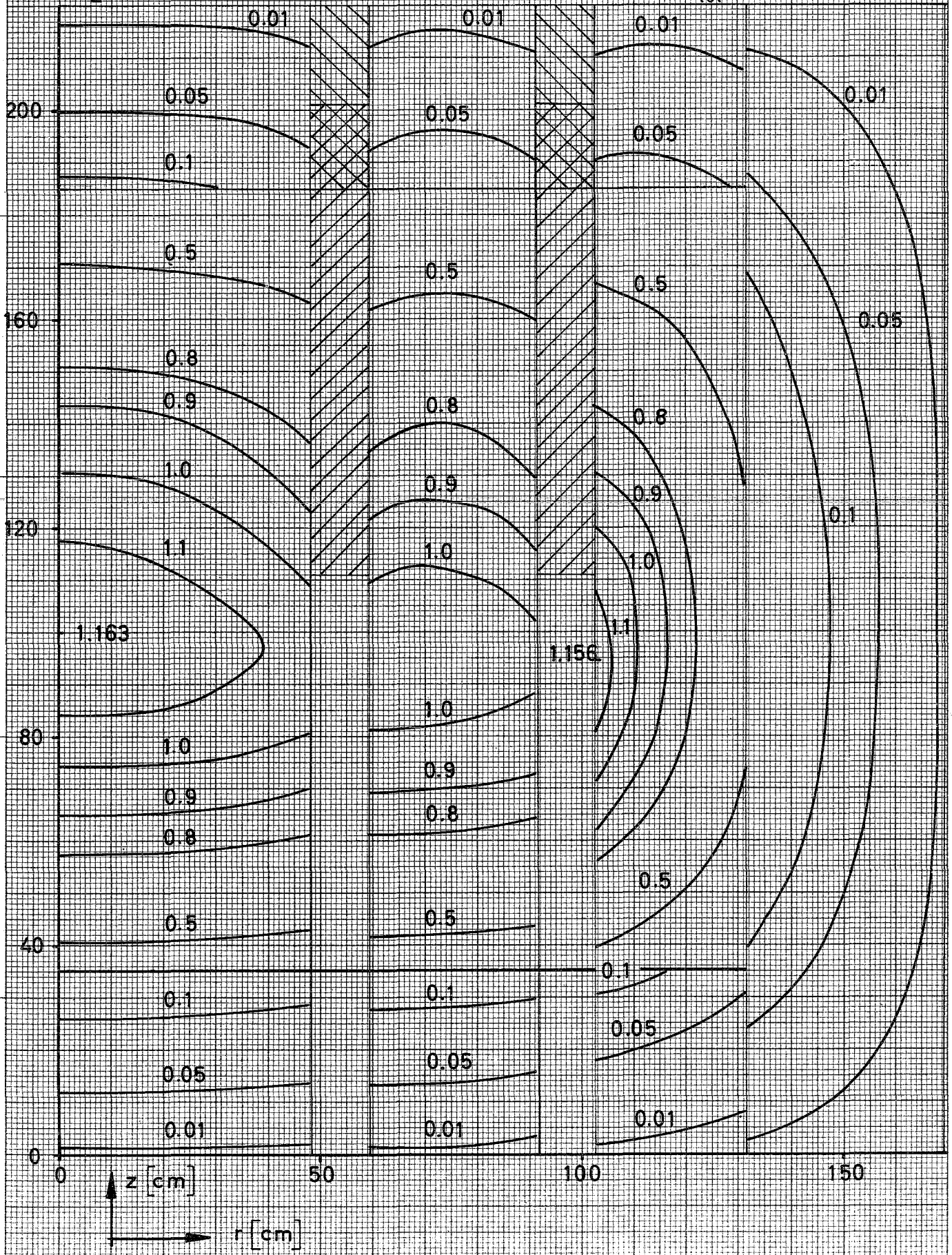


Fig. 3.9. Fission distribution as function of the azimuthal angle for different radii Case : $N_1 = 0$, $N_2 = 6$

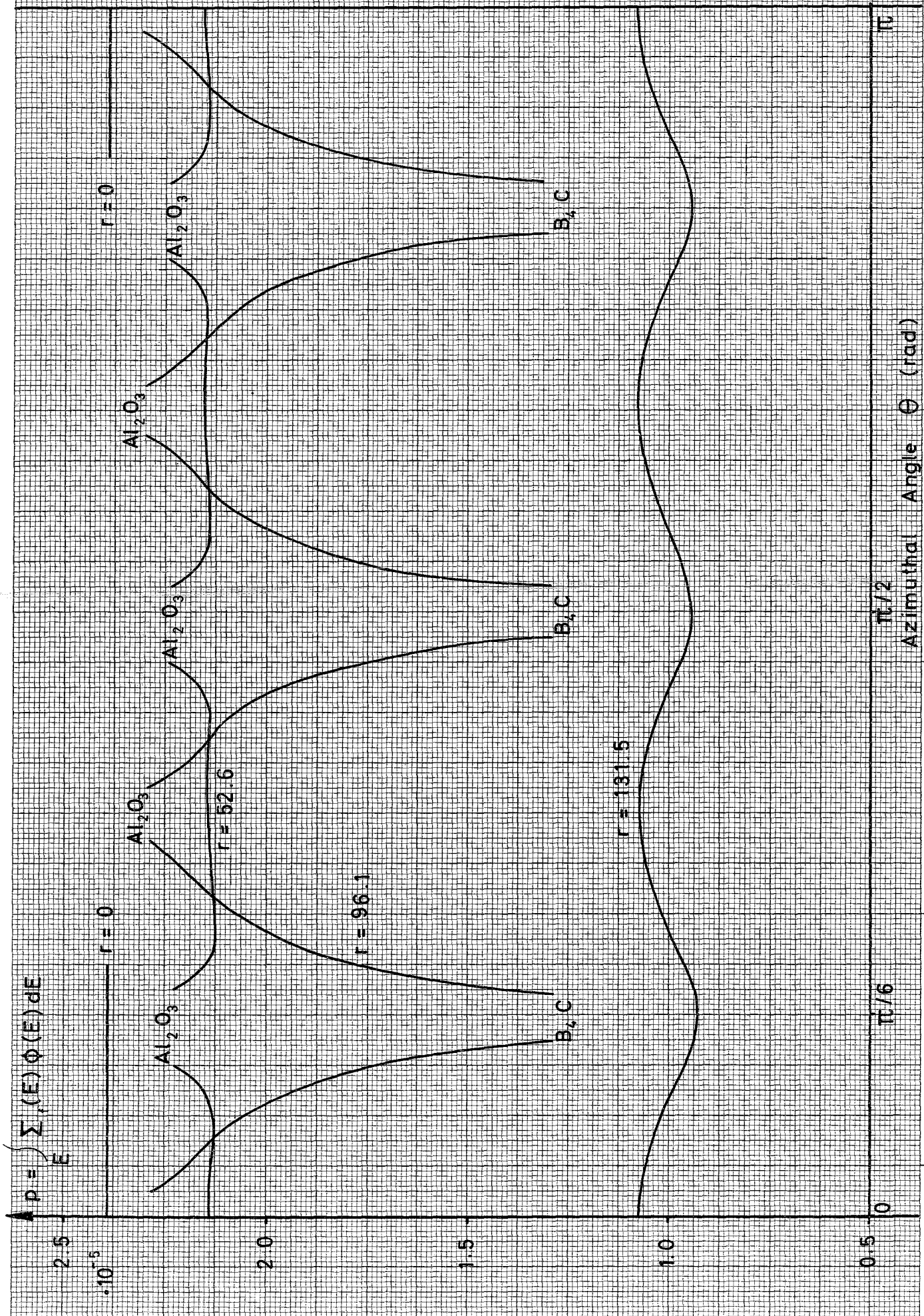


Fig. 3.10 Fission distribution as function of the azimuthal angle for different radii Case: $N_1 = 6$, $N_2 = 0$

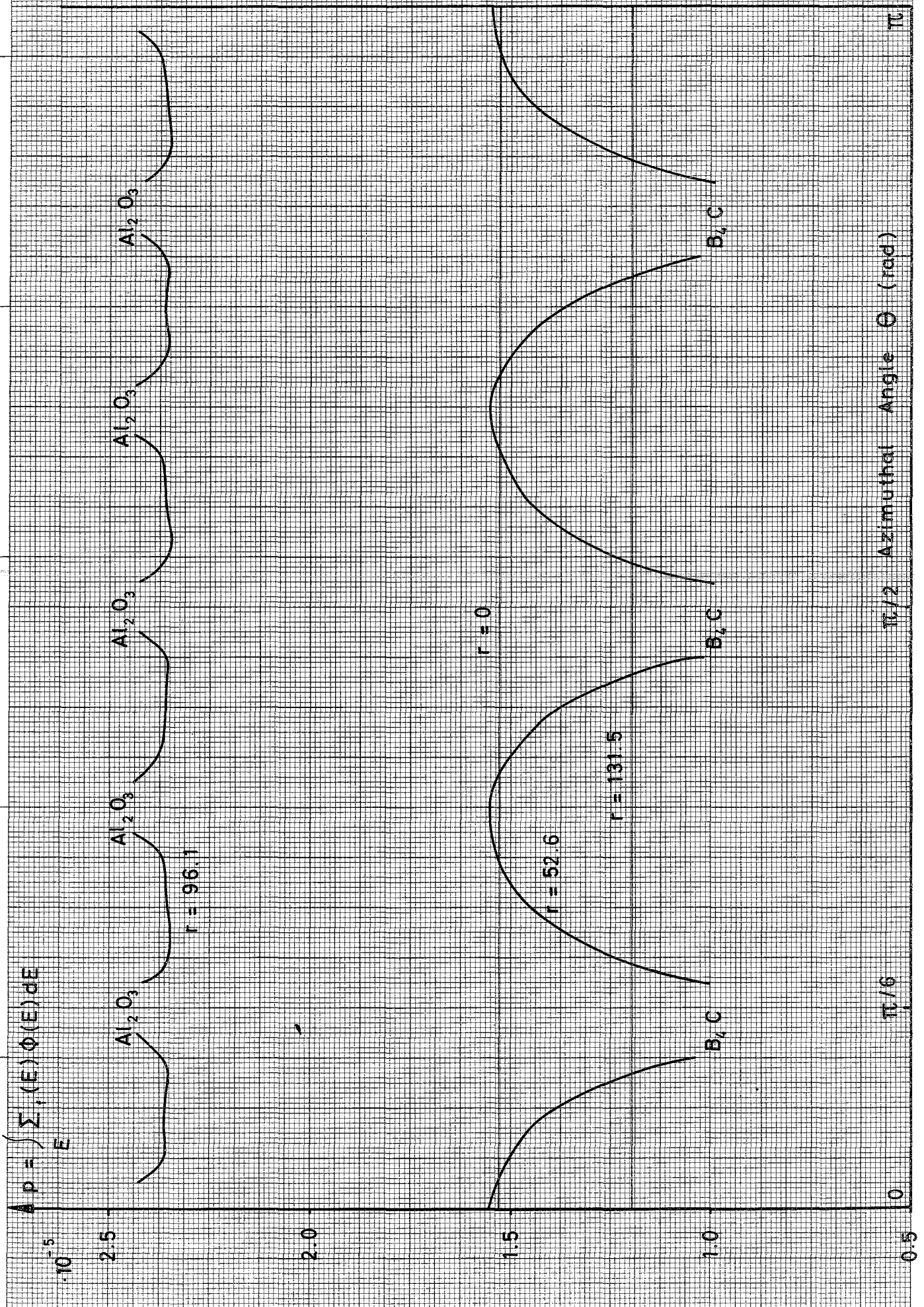


Fig 3.11. Two-dimensional fission distribution in $(r - \theta)$ geometry

Case: $N_1 = 6$, $N_2 = 0$

